Analysis of vapor phase reaction by high-resolution mass spectrometry for Group III-Nitrides epitaxial growth

YE Zheng

Analysis of vapor phase reaction by high-resolution mass spectrometry for Group III-Nitrides epitaxial growth

YE Zheng

Nagoya University

Graduate School of Engineering

Department of Electrical Engineering and Computer Science

高分解能質量分析によるIII族窒化物半導体気相成長の解析

叶　正

名古屋大学大学院

工学研究科

電子情報システム専攻電子工学分野

ABSTRACT OF THIS THESIS

Title: Analysis of vapor phase reaction by high-resolution mass spectrometry for Group III-Nitrides epitaxial growth

YE Zheng

Thesis Advisor: Professor Hiroshi Amano

In this thesis, the main objective is to explore specific processes in gas phase reactions of GaN growth by metalorganic vapor phase epitaxy (MOVPE). Our approach is to introduce a high-resolution (about 0.002 u) time-of-flight mass spectrometry (Tof-MS) system to analyze the gas phase reaction. First, the reliability of the mass spectrometer was tested. ToF-MS proved to be suitable for the analysis of complicated MOVPE gas-phase reactions through the detection results of a conventional quadrupole mass spectroscopy (QMS) and the actual observation experiments introduced into the actual reactor. A simple reactor was built to make experiments more convenient. In the MOVPE growth mode, trimethylgallium (TMGa) and ammonia (NH_3) are used as gallium precursor and nitrogen precursor for GaN, respectively. Compared with the complex reaction of directly detecting the actual growth, the measurement of the individual decomposition process of each raw material is more helpful to our understanding of the MOVPE reaction mode. The decomposition process of NH_3 under nitrogen was observed first. Even at the high temperature of 1200 °C (Flow rate: 0.02m/s), only 26% of NH_3 decomposed in a clean metal-free reactor, whereas a higher ratio of NH_3

decomposition was realized in the presence of stainless steel. Subsequently, the decomposition process of TMGa under different carrier gases was studied. TMGa begins to decompose in hydrogen (H_2) and nitrogen (N_2) at 375 and 520 °C, respectively. In contrast to the almost inert N_2, H_2 participates in the reaction. the H_2 carrier gas can produce active H* owing to thermal dissociation above 350 ℃, which is due to the high-energy tail of the Maxwell-Boltzmann distribution. Therefore, TMGa is not decomposed by thermal collision in H_2 atmosphere instead active H* attaches to the CH_3 groups of $Ga(CH_3)_3$ and forms the main product CH_4 above 400 ℃. In contrast, the strong signal of CH_3 suggest the $Ga(CH_3)_3$ loses CH_3* via thermal decomposition in N_2 atmosphere. Specifically, in the nitrogen atmosphere, with the decomposition of TMGa, we observed high-intensity signal of hydrocarbons compounds such as ethane (C_2H_6) and ethylene (C_2H_4). Finally, by introducing pure C_2H_6, TMG was proved preferentially generates C_2H_6 during the thermal decomposition process. We also observed that C_2H_6 will continue to decompose into C_2H_4 and acetylene (C_2H_2) at high temperatures. However, In the presence of NH_3, hydrocarbon compounds (even CH_4) will react with NH_3 to form HCN. This type of reaction mode was first reported to occur during the gas phase reaction of nitrides. HCN is not only highly toxic but can also be used as a carbon doping material for GaN. While calling on all operators of nitride crystal growth to pay more attention to safety, whether HCN is the main source of unintentional carbon doping needs to be carefully explored. However, by comparing the reactions at different flow rates, I eventually found that unintentionally doped carbon sources were more likely to come

from undecomposed metalorganics.

CONTENTS

Chapter 1 Introduction & research objective

1.1 Introduction

It is expected that energy consumption will continue to increase due to social development and population growth. As shown in Fig. 1.1, electricity used in daily life is obtained by converting energy mainly from fossil fuels (i.e., coal, oil, and natural gas). Since the energy used depends heavily on fossil fuels, the problem of energy shortages must be seriously considered. According to predictions on how many years to use primary energy resources, even if energy consumption does not increase, oil is expected to last for about 40 years, about 66 years have been reported for natural gas, about 60 years for uranium, and about 150 years for coal [1]. Many measures have been proposed to mitigate the depletion of energy resources, including the development of new energies, renewable energies, and the development of energy-saving technologies. However, although the introduction of new energy is expected, sufficient energy has not yet been obtained due to low energy conversion efficiency and equipment utilization rate and high cost. Therefore, it is required to efficiently use limited energy resources in order to continue the development and living of economic activities.

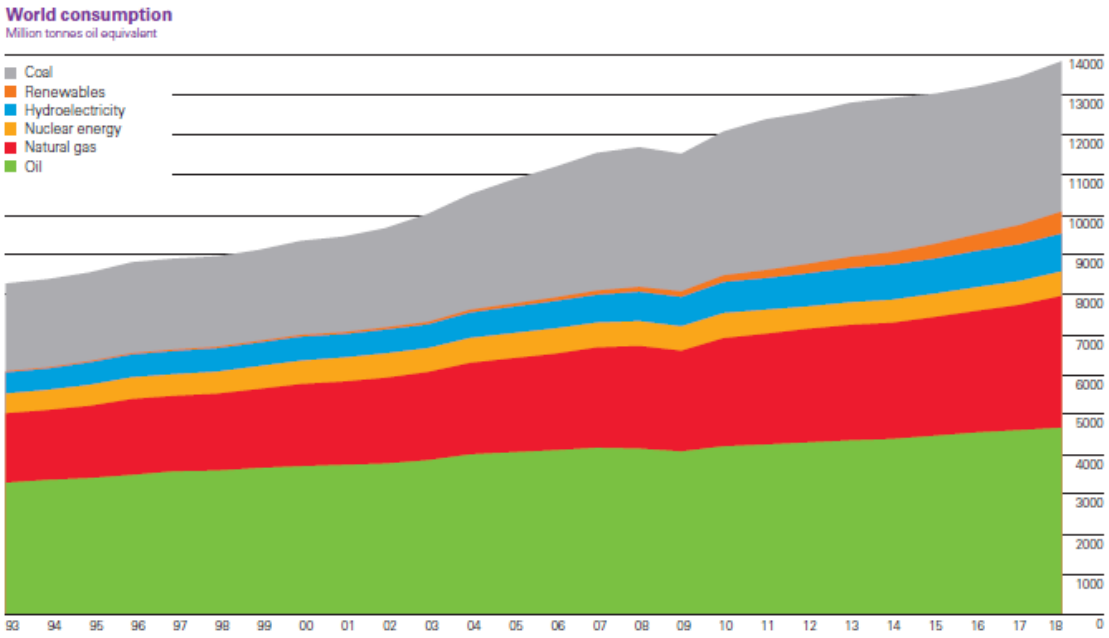

Figure 1.1 Primary energy: consumption by fuels [2].

In 1947, Bell Labs' Walter Brattain, John Bardeen, and William Bradford Shockley invented the world's first transistor with Ge-based amplification [3,4]. In 1959, Jack St. Clair Kilby introduced an integrated circuit (IC) on Ge substrate [5], and then Robert Norton Noyce invented it using a Si substrate. After that, microfabrication technology and high integration technology for devices mainly using Si with the development of the semiconductor device, the integration of semiconductor devices has been remarkably increased. While Si-based devices have developed for information processing applications, Si semiconductor have also developed as power devices for controlling high power. Thyristors were first developed and commercialized as power semiconductors in

1957. Since then, IGBTs (Insulated Gate Bipolar Transistors) that have the advantages of thyristors and Metal-Oxide-Semiconductor field-effect transistors (MOSFETs) and super junction MOSFETs (SJ-MOSFETs) have been developed [6]. Is the mainstream of power semiconductors. Power semiconductors have been improved in switching speed and low loss with the advance of the technology, and the range of use thereof has been expanding. However, on the other hand, since the element is responsible for power conversion, further lower loss is required, but the Si-based device has reached its limit due to the physical properties of Si. Even though the Si-based device performance beyond the limits of Si by applying complex structure [7,8], application of new materials is still expected. Accordingly, great expectations are placed on compound semiconductor materials which are more excellent in material properties as elements for power semiconductors than Si. Group-III nitrides semiconductors have properties such as a wide band gap, high breakdown electric field, and low on-resistance, and are expected to be applied to higher-temperature operation, higher breakdown voltage, and lower loss than Si-based devices.

1.2 Group-III nitride semiconductor

Group-III nitrides including AlN, GaN, InN and their alloys has been intensively studied. Table 1.1 shows properties of some common semiconductor materials. Group III nitride semiconductors have a direct band structure and can be made of ternary and

quaternary mixed crystals (AlGaN, InGaN, AlInN, AlGaInN), so the energy band gap can be change from about 0.6 to 6.2 eV. Therefore, it is considered possible to cover the entire visible light region, and from infrared to deep ultraviolet. Obviously, due to this characteristic, GaN plays an irreplaceable role in the application of light emitting devices (LED).Additionally, GaN is also an ideal material for the development of high-power devices owing to the its excellent properties, such as a direct wide bandgap, high dielectric breakdown electric field, high chemical and thermal stability.

Table 1.1: Properties of some semiconductor materials at room temperature [9-16].

	Bandgap (eV)	Electron mobility (cm^2/Vs)	Electric breakdown field ($10^6V/cm$)	Saturated electron velocity ($10^7cm/s$)	Thermal conductivity (W/cmK)
AlN	6	-	-	2.5	2.1
Diamond	5.47	2200	10	3	20
β-Ga_2O_3	4.8-4.9	300	8	1.3	0.136 [100] 0.228 [010]
GaN	3.39	900 2DEG:1500	3.3	2.5	1.3
4H-SiC	3.23	900	3.23	2	4.9
GaAs	1.43	8500 2DEG:10000	0.4	1	0.5
Si	1.12	1500	0.3	1	1.5
InN	0.6-0.7	4000	2	4.2	0.8

As shown in the various physical properties arranged in table 1.1, wide band gap (WBG) semiconductor materials have superior properties, especially β-Ga_2O_3 and diamond. The

low thermal conductivity of β-Ga_2O_3 results in the need for additional heat management solutions to maintain the performance and reliability of power device [17,18]. Due to the influence of scattering, β-Ga_2O_3 electron mobility is also very low [19]. The above characteristics limited the application of β-Ga_2O_3 in high-voltage and high-current power equipment. Diamond is also unable to take advantage of its current performance characteristics due to the lack of homoepitaxial diamond substrates [20,21] and effective N-type doped materials [22,23]. Compared to β-Ga_2O_3 and diamond, which are still in the early stages of research, the development of SiC and GaN has entered a period of practical use. SiC has begun to be installed on cars and railway vehicles. Development of GaN has been delayed due to difficulties in growing crystals, but intensive research is currently being conducted toward the application of power devices.

GaN is a representative of Group III nitride semiconductors, is a WBG semiconductor compared to Si. So inter-band transition of electrons due to generated thermal energy is unlikely to occur, and stable operation is possible even at a high temperature which cannot be driven by other semiconductor materials such as Si. For this reason, nitride semiconductors are expected to be applied to devices where high-temperature operation is required. Also, because of it is resistant to heat, cooling of an apparatus using a GaN power device can be simplified. Since a heterostructure having band discontinuity can be formed between AlGaN and GaN, a two-dimensional electron gas having a large electron concentration is formed due to strong piezoelectricity and spontaneous polarization at the

interface of the heterostructure. Further, due to the nitride semiconductor is characterized by a high electron saturation speed and a high electron mobility, it is considered that a heterojunction field effect transistor having a large current and a high-speed switching operation can be obtained. The high-speed switching operation makes it possible to reduce the switching loss of the power device. Also, because of the large breakdown electric field, GaN-based devices can be expected to have higher withstand voltage characteristics for devices of the same size as Si-based devices. The lower the on-resistance, the lower the heat generation during the on operation of devices [24]. Equation 1.1 indicates that the on-resistance that causes heat loss during power conversion is inversely proportional to the cube of the dielectric breakdown electric field. Since the breakdown electric field of GaN is about 10 times greater than that of Si, an extremely low on-resistance of about 1/1000 of Si can be expected. Therefore, it leads to reduction of heat loss, and energy can be saved as a power device. In addition, nitride semiconductors are made of environmentally friendly and highly safe materials and have excellent properties such as mechanical stability and chemical stability due to the strength of bonding between atoms. In future, the vast expansion of the application fields of the GaN devices are expected.

$$R_{on} = \frac{4{V_B}^2}{\varepsilon \mu_n} \cdot \frac{1}{{E_c}^3} \tag{1.1}$$

(V_B: breakdown voltage, R_{on}: on-resistance, ε: dielectric constant, μ_n: electron m

obility, E_c: breakdown electric field)

As described above, nitride semiconductor materials have excellent physical properties such as wide band gap, high breakdown electric field, and low on-resistance. If these physical properties are utilized, on-loss and switching loss are smaller than Si power devices. Application to power devices that operate at high temperatures, withstand high voltages, and have low losses is greatly expected. Furthermore, there is an advantage that the device can be reduced in size and thickness.

1.2.1 History of high-quality GaN crystals

In order to realize the device, it is essential to produce high quality crystals. However, group III nitride semiconductors have an extremely high melting point and a high equilibrium vapor pressure of nitrogen at the growth temperature, making it difficult to produce bulk single crystals such as AlN, GaN, and InN from melts like Si [25]. At present, Group III nitride semiconductor has been applied in various applications, but practically there have been many difficulties in practical. One of them is that it was difficult to produce high quality crystals. In epitaxial growth, it is common to select a substrate of the same type or a substrate that is lattice-matched as a substrate crystal serving as a base. However, since a group III nitride semiconductor single crystal does not exist in nature and there is no lattice matching substrate crystal, it is necessary to perform heteroepitaxial growth on a substrate having a large lattice mismatch such as sapphire. In 1969, Maruska

et al. succeeded in producing a GaN single crystal on a sapphire substrate by the halide vapor phase epitaxy (HVPE) method [26], but the GaN crystal at that time had very many surface irregularities and cracks. High quality crystals were not obtained. In addition, high-density dislocations are generated in the crystal due to lattice mismatch, and the residual donor concentration becomes extremely high. From the above, it has been considered that it is impossible to realize a blue light emitting device using Group III nitride semiconductor. However, in 1986, Amano et al. used metal organic vapor phase epitaxy (MOVPE) to deposit a thin layer of AlN on sapphire as a buffer layer at low temperature and growth GaN on it, found that mismatch of heterogeneous substrate could be mitigate [27]. As a result, it was possible to produce a colorless, transparent and mirror-like crystal with no cracks or pits and few crystal defects and succeeded in dramatically improving the crystallinity of GaN. After that, p-type conductivity in Mg-doped GaN via low-energy electron beam irradiation (LEEBI) was realized in 1989 and Amano et al. successfully demonstrated the first GaN p-n junction blue LED [28]. Based on these results, research on nitride semiconductors has made great progress. In 1991, Nakamura et al. commercialized a blue LED using InGaN by fabricating a double heterostructure [28], and in 1995 developed an InGaN multiple quantum well structure [29]. The high-brightness blue LED used was put to practical use. At present, blue LEDs are used n LED bulbs because they can emit white light when combined with yellow phosphors, and they can reduce power consumption significantly compared to light sources using

conventional incandescent bulbs.

1.2.2 GaN power device applications

As described above, GaN, which is widely used as a light emitting device, is also excellent as a power semiconductor or high-frequency semiconductor material because it has a wide band gap, a high breakdown electric field, and a high saturation electron velocity.

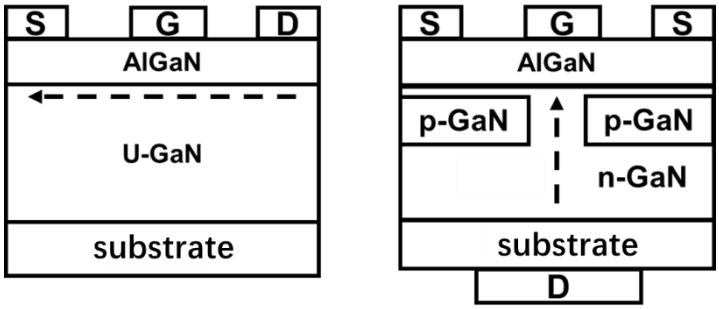

Figure 1.2 Simplified cross-sectional view of horizontal and vertical device structures.

As show in Fig 1.2, power devices are classified into two types: horizontal devices in which the drift region is formed parallel to the substrate surface, and vertical devices in which the drift region is formed perpendicular to the substrate surface [30]. As a lateral device in nitrides semiconductor, a high electron mobility transistor (HEMT) using a

heterostructure of AlGaN and GaN is generally used. When an AlGaN layer having a smaller lattice constant than GaN is grown thereon, tensile stress occurs in the AlGaN layer, and piezoelectric polarization occurs in the AlGaN layer. Due to these spontaneous polarization and piezoelectric polarization, positive fixed charges are generated at the AlGaN / GaN heterojunction interface, and a triangular potential quantum well is formed on the GaN side. Therefore, a high-concentration two-dimensional electron gas is generated at the AlGaN / GaN hetero interface without doping with impurities. HEMTs use this two-dimensional electron gas and have applications as DC / DC converters as high-frequency devices due to their extremely high channel mobility and low on-resistance [31]. However, it is difficult to operate at a large current, and there are disadvantages such as an increase in the element area as the withstand voltage is increased. Therefore, low voltage applications up to about 600 V are desired.

Vertical devices tend to have a higher breakdown voltage structurally than horizontal devices, and the breakdown voltage can be controlled by the thickness of the drift layer. Since a large current density per area can be obtained, a device capable of operating at a high withstand voltage and a large current can be expected. Since GaN initially did not have a conductive substrate, research on horizontal devices was focused on, but with the advancement of GaN bulk substrate fabrication technologies such as the HVPE method, Ammonothermal method [32], and Na flux method [33], vertical device production has become possible. In recent years, excellent results such as a pn junction diode with a

withstand voltage of about 3.7 kV [34] and a trench gate MOSFET with a withstand voltage of about 1600 V have been reported [35], and research on GaN vertical devices has been actively conducted.

1.2.3 Epitaxial growth technology for III-nitride semiconductor device

Generally, the epitaxial growth of the GaN power device structure is performed by the MOVPE method. A schematic diagram of a general MOVPE method is shown in Fig 1.3. The MOVPE method is a method using an organometallic compound such as trimethylgallium (TMGa: $Ga(CH_3)_3$) or trimethylaluminum (TMAl: $Al(CH_3)_3$). A nitride semiconductor crystal can be epitaxially grown by a thermal decomposition reaction of an organometallic compound as a Group III material and NH_3 as a Group V material on a heated substrate. The overall reaction process in MOVPE can be divided into two parts, a gas phase reaction and a surface reaction. The raw materials transported to the heating zone by the carrier gas reacted in the gas phase, and finally crystallized on the surface of the substrate [36]. In the MOVPE method, the growth rate is determined only by the supply amount of the group III raw material, and by controlling the gas flow rate, the film thickness can be controlled in a wide range from an extremely thin film of about several nm to a relatively thick film of about several μm. It is easy to produce a complicated multilayer structure and a steep hetero interface. Also, the composition control and the

doping concentration control of the alloys can be controlled by the gas flow rate. Furthermore, it is also excellent in that the in-plane uniformity is good and the area can be increased. From these characteristics, most of the GaN power device structures are currently manufactured by the MOVPE method.

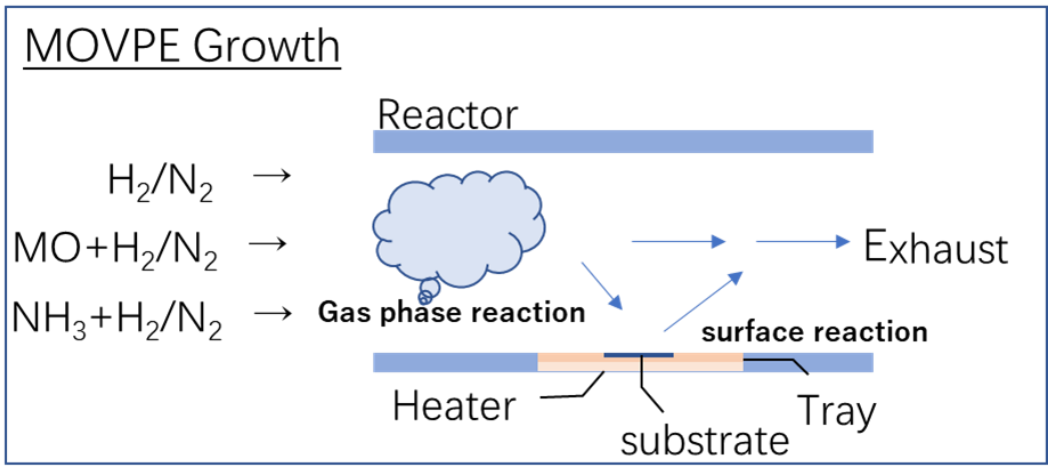

Figure 1.3 Schematic of MOVPE growth method

However, the MOVPE method has some drawbacks in increasing the breakdown voltage of power devices. One is that the growth rate is slow. From Fig 1.4, in the vertical device, it is necessary to design the drift layer, which is the breakdown voltage maintaining layer, to have a sufficiently large thickness in order to increase the breakdown voltage. However, the MOVPE method is difficult because the growth rate is as slow as several μm / h at the maximum, and it takes a long time to grow a thick film exceeding 10 μm. The second is the contamination of crystals with impurities. In general, in GaN

growth, even if an undoped crystal contains unintentional residual impurities [38], it may act as a donor or an acceptor [39]. However, according to Fig 1.3, a drift layer having a low impurity concentration is required to increase the breakdown voltage of the device, and it is essential to control the residual impurity concentration to 10^{14} cm^{-3} or less to achieve breakdown voltage of 10 kV [40]. Since the MOVPE method is a growth method using an organic metal compound as a raw material, it is inevitable that carbon is mixed into the crystal. It is known that carbon in GaN forms a deep acceptor level or a shallow donor level [39,40], and it is difficult to control the carrier concentration. Therefore, it is essential to reduce the carbon concentration in the drift layer.

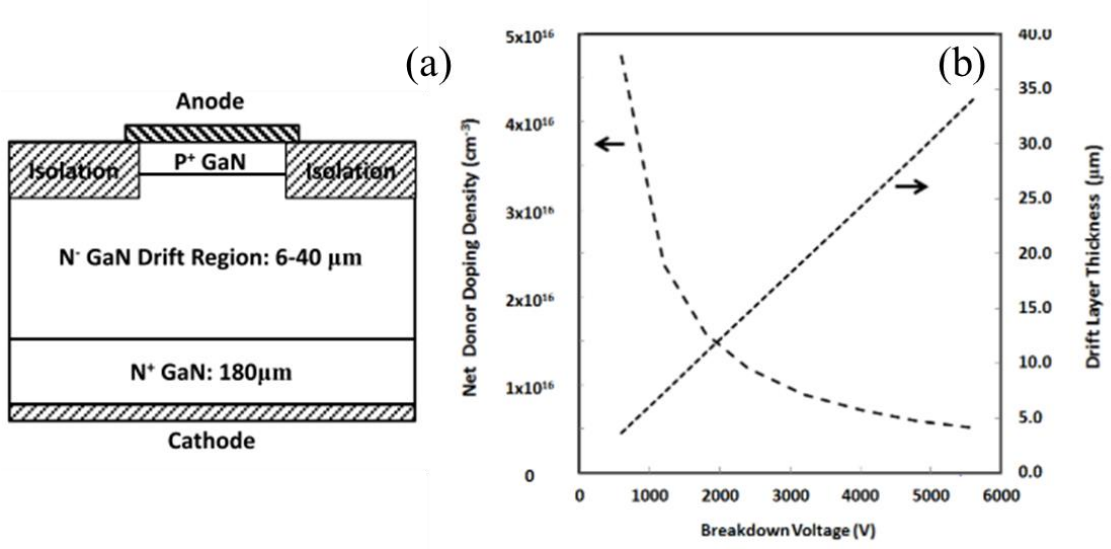

Figure 1.4 (a)Schematic of a vertical GaN p-n diode highlighting critical features; (b) Optimum design of GaN vertical device as guided by FOM [37].

For mass production of high-performance power devices, reducing unintentional

carbon incorporation into thick drift layers in vertical GaN-based devices are required. There are many reports which investigated the relationships between growth conditions and C incorporation in GaN. It is known that growth conditions can affect to reduce unintentional doped C concentration including high growth temperature [41], high V/III ratio [42-47], low growth rate [47] and high growth pressure [48]. However, reducing the carbon concentration is especially difficult under the optimized growth conditions, because carbon is the constituent element of TMGa which provides the methyl group in the production process. Until now, there are still no reports about effectively reduce the concentration of unintentionally doped C concentration to 10^{14} cm^{-3}. Furthermore, C incorporation mechanisms or physical backgrounds of these phenomena, however, are still unclear. For practical purposed such as reducing unintentional carbon incorporation into thick drift layers in vertical GaN-based devices require a better understanding of the organometallic chemistry.

1.3 Gas phase analysis technology

As we mentioned before, the overall reaction process in MOVPE can be divided into two parts, a gas phase reaction and a surface reaction, and reactions in the gas phase occur preferentially. Therefore, to obtain an in-depth understanding of the entire reaction process in MOVPE, the analysis of the gas phase reaction is crucial to the clarification of

the overall reaction and the realization of theoretical calculations.

There are many test methods regarding the detection of reactions in the gas phase, such as chemical titration [49], Fourier transform infrared spectrometry (FTIR) [50-55], and quadrupole mass spectrometry (QMS) [56-59], have been commonly used in the previous studies. However, the typical flow speed of up to a few meters per second in MOVPE corresponds to gas residence times in the hot zone on the order of seconds rather than minutes. Therefore, non-equilibrium reaction detection method is required. Moreover, because there may be a small number of unknown products (below PPM), a high resolution and high sensitivity measurement method is necessary. Taken together, mass spectrometry (MS) may be appropriate for our purposes. MS is an analytical technique that measures the mass-to-charge ratio of ions. The results are typically presented as a mass spectrum, a plot of intensity as a function of the mass-to-charge ratio. Mass spectrometry is used in many different fields and is applied to pure samples as well as complex mixtures. A mass spectrum is a plot of the ion signal as a function of the mass-to-charge ratio. These spectra are used to determine the elemental or isotopic signature of a sample, the masses of particles and of molecules, and to elucidate the chemical identity or structure of molecules and other chemical compounds. A mass spectrometer consists of three components: an ion source, a mass analyzer, and a detector. The ionizer converts a portion of the sample into ions. There is a wide variety of ionization techniques, depending on the phase (solid, liquid, gas) of the sample and the efficiency of various

ionization mechanisms for the unknown species. An extraction system removes ions from the sample, which are then targeted through the mass analyzer and into the detector. The differences in masses of the fragments allows the mass analyzer to sort the ions by their mass-to-charge ratio. The detector measures the value of an indicator quantity and thus provides data for calculating the abundances of each ion present. Some detectors also give spatial information. For a conventional quadrupole mass spectrometer (QMS), the mass resolution is only 1 u (u: unified atomic mass unit). During the growth process of GaN, here are many components of similar masses, such as N_2 and C_2H_4 which have masses of 28.006 u and 28.031 u, respectively (Some products of similar quality were sorted into the table 1.2). To a better understanding of the entire reaction process in MOVPE, the time-of-flight mass spectrometry (TOF-MS) has recently been introduced for in situ gas phase monitoring.

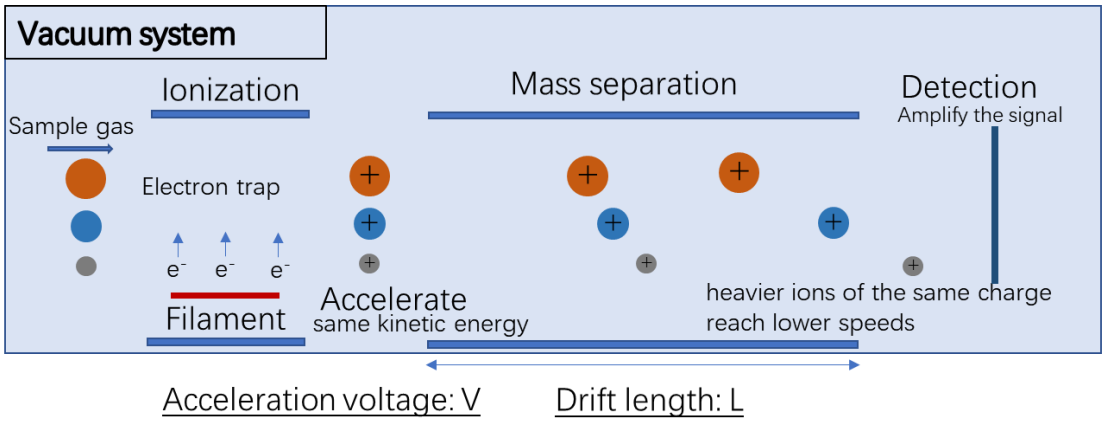

Figure 1.5 Schematic diagram of time-of-flight mass spectrometry

Schematic diagram of TOF-MS was show in Fig 1.5. The principle of time-of-flight mass spectrometer is as follows:

Independent of the ionization method, the electric charge q of an ion of mass m is equal to an integer number z of electron charge e, that is $q = ez$. The ene rgy uptake E by moving through a voltage V is given by

$$E = qV = ezV \tag{1.2}$$

Thereby, the former potential energy of a charged particle in an electric field is converted into kinetic energy

$$E = ezV = \frac{1}{2}mv^2 \tag{1.3}$$

The ion will have velocity

$$v = \left(\frac{2zeV}{m}\right)^{1/2} \tag{1.4}$$

that depends on its mass. The time (T) required to traverse the drift length L

$$T = \left(\frac{m}{2ezV}\right)^{1/2} L \tag{1.5}$$

also depends on the mass of the ion, so that the time spectrum can be converted directly to

a mass spectrum

$$\frac{m}{z} = 2eV\left(\frac{T}{L}\right)^2 \tag{1.6}$$

To obtain timing information, the time of ion extraction (or formation) must be

known. Thus, TOF mass spectrometers generally use pulsed extraction (or ionization). The time interval between ion extraction (or ionization) and detection is measured as time (t). The entire time/amplitude record is digitized by an analog-to-digital converter.

Table 1.2 Some products of similar mass that may appear

Products	Mass (u)	Products	Mass (u)	Products	Mass (u)
N	14.00307	H_2O	18.01056	HCN	27.0109
CH_2	14.01565	$^{15}NH_3$	18.02358	C_2H_3	27.02348
NH	15.0109	NH_4	18.03437	N_2	28.00615
CH_3	15.02348	CH_2D_2	18.04385	HCNH	28.01872
NH_2	16.01872	CHD_3	19.05013	C_2H_4	28.0313
CH_4	16.0313	CD_4	20.05641	$^{29}N_2$	29.00318
OH	17.00274	CN	26.00307	N_2H	29.01397
NH_3	17.02655	C_2H_2	26.01565	C_2H_5	29.03913
CH_3D	17.03758			C_2H_6	30.04695

1.4 Research objectives and synopsis

With the increasing application prospects of Group-III nitride semiconductor, the principle of crystal growth needs to be elaborated (for example: unintentional incorporation of carbon in GaN). Although the crystal quality can be improved by optimizing the crystal growth conditions, the reaction inside the reactor is still unclear. To the realization of high-quality materials for extended nitride semiconductors application, the main objectives of this research is to explore specific processes in gas phase reactions of GaN MOVPE.

This thesis is composed of six chapters.

In Chapter 1, many researchers are paying attention to nitride power devices that can realize higher breakdown voltage and lower loss than Si-based devices in order to efficiently use limited energy resources. For a GaN vertical power device with a large current and a high breakdown voltage, crystal growth of a low-concentration impurity is required. However, it was found that it is important to reduce unintentional carbon contamination due to insufficient decomposition of the organometallic raw material during GaN epi growth. This chapter describes the background and purpose of this study.

In Chapter 2，experimental equipment and some preliminary results will be introduced.

In Chapter 3, the decomposition of NH_3 in N_2 ambient was studied under non-equilibrium conditions similar to those in a MOVPE reactor during the epitaxial growth of group-III nitrides.

In Chapter 4, we examined the decomposition of TMGa in H_2 and N_2 atmospheres at first.

In Chapter 5, the reaction between TMGa and NH_3 is clarified. I have discovered that a large amount of HCN is produced in the gas phase, and the principle of its formation will be discussed in detail. The possibility of Ga catalysts is also mentioned in this chapt er. Finally, in order to approximate the conditions of a real reactor, the relationship betw een the gas phase reaction and the flow rate will be discussed.

In Chapter 6, I summarize the results obtained in this study and discuss future issues

and prospects.

1.5 References

[1] 西岡 秀三, 村野 健太郎, 宮﨑 忠國 編著: [改訂新版] 地球環境がわかる技術評論社, 2015.

[2] BP p.l.c, BP Statistical Review of world Energy, London, United Kingdom, 2019.

[3] W. Shockley, US Patent US2502448, 1948.

[4] J. Bardeen, and W. H. Brattain, US Patent US2524035, 1948.

[5] J. S. Kilby, "Invention of the integrated circuit," *IEEE Trans. Electron Devices*, vol. 23, no. 7, pp. 648–654, Jul. 1976.

[6] A. Griffoni et al., "Neutron-induced failure in silicon IGBTs, silicon super-junction and SiC MOSFETs," IEEE Trans. Nucl. Sci., vol. 59, no. 4 PART 1, pp. 866–871, 2012.

[7] W. Saito, I. Omura, T. Ogura, and H. Ohashi, "Theoretical limit estimation of lateral wide band-gap semiconductor power-switching device," *Solid. State. Electron.*, vol. 48, no. 9, pp. 1555–1562, 2004.

[8] A. Nakagawa, "Theoretical investigation of silicon limit characteristics of IGBT," *Proc. Int. Symp. Power Semicond. Devices ICs*, vol. 2006, pp. 4–7, 2006.

[9] M. E. Levinshtein, L. S. Rumyantsev, M. S. Shur, "Properties of Advanced Semi conductor Materials: GaN, AIN, InN, BN, SiC, SiGe", John Wiley & Sons, 2001.

[10] L. M. Tolbert, B. Ozpineci, S. K. Islam, and M. S. Chinthavali, "Wide bandgap semiconductors for utility applications," in *Proceedings of the IASTED Multi-Conference- Power and Energy Systems*, 2003, vol. 7, pp. 317–321.

[11] K. Shenai, R. S. Scott, and B. J. Baliga, "Optimum semiconductors for high-power electronics," *IEEE Trans. Electron Devices*, vol. 36, no. 9, pp. 1811–1823, 1989.

[12] R. T. Kemerley, H. B. Wallace, and M. N. Yoder, "Impact of wide bandgap microwave devices on DoD systems," *Proc. IEEE*, vol. 90, no. 6, pp. 1059–1064, 2002.

[13] U. K. Mishra, Shen Likun, T. E. Kazior, and Yi-Feng Wu, “GaN-Based RF Power Devices and Amplifiers,” *Proc. IEEE*, vol. 96, no. 2, pp. 287–305, Feb. 2008.

[14] H. W. Xue, Q. M. He, G. Z. Jian, S. B. Long, T. Pang, and M. Liu, “An Overview of the Ultrawide Bandgap Ga2O3 Semiconductor-Based Schottky Barrier Diode for Power Electronics Application,” *Nanoscale Res. Lett.*, vol. 13, pp. 1–13, 2018.

[15] P. J. Wellmann, “Power Electronic Semiconductor Materials for Automotive and Energy Saving Applications – SiC, GaN, Ga2O3, and Diamond,” *Zeitschrift fur Anorg. und Allg. Chemie*, vol. 643, no. 21, pp. 1312–1322, 2017.

[16] M. Kim, J. H. Seo, U. Singisetti, and Z. Ma, “Recent advances in free-standing single crystalline wide band-gap semiconductors and their applications: GaN, SiC, ZnO, β-Ga 2 O 3 , and diamond,” *J. Mater. Chem. C*, vol. 5, no. 33, pp. 8338–8354, 2017.

[17] Z. Guo *et al.*, “Anisotropic thermal conductivity in single crystal β-gallium oxide,” *Appl. Phys. Lett.*, vol. 106, no. 11, pp. 1–6, 2015.

[18] M. D. Santia, N. Tandon, and J. D. Albrecht, “Lattice thermal conductivity in β - Ga 2 O 3 from first principles,” *Appl. Phys. Lett.*, vol. 107, no. 4, 2015.

[19] N. Ma *et al.*, “Intrinsic electron mobility limits in β-Ga2O3,” *Appl. Phys. Lett.*, vol. 109, no. 21, pp. 1–6, 2016.

[20] J. Isberg *et al.*, “High carrier mobility in single-crystal plasma-deposited diamond,” *Science (80-.).*, vol. 297, no. 5587, pp. 1670–1672, 2002.

[21] J. Isberg, J. Hammersberg, D. J. Twitchen, and A. J. Whitehead, “Single crystal diamond for electronic applications,” *Diam. Relat. Mater.*, vol. 13, no. 2, pp. 320–324, 2004.

[22] S. Koizumi, K. Watanabe, M. Hasegawa, and H. Kanda, “Formation of diamond p-n junction and its optical emission characteristics,” *Diam. Relat. Mater.*, vol. 11, no. 3–6, pp. 307–311, 2002.

[23] M. Katagiri, J. Isoya, S. Koizumi, and H. Kanda, “Lightly phosphorus-doped homoepitaxial diamond films grown by chemical vapor deposition,” *Appl. Phys.*

Lett., vol. 85, no. 26, pp. 6365–6367, 2004.

[24] 赤﨑 勇　編著:　III-V族化合物半導体, 培風館, 2004.

[25] J. Karpiński, J. Jun, and S. Porowski, “Equilibrium pressure of N2 over GaN and high pressure solution growth of GaN,” *J. Cryst. Growth*, vol. 66, no. 1, pp. 1–10, 1984.

[26] H. P. Maruska and J. J. Tietjen, “The preparation and properties of vapor-deposited single-crystal-line GaN,” *Appl. Phys. Lett.*, vol. 15, no. 10, pp. 327–329, 1969.

[27] H. Amano, N. Sawaki, I. Akasaki, and Y. Toyoda, “Metalorganic vapor phase epitaxial growth of a high quality GaN film using an AlN buffer layer,” *Appl. Phys. Lett.*, vol. 48, no. 5, pp. 353–355, 1986.

[28] H. Amano, M. Kito, K. Hiramatsu, and I. Akasaki, “P-Type Conduction in Mg-Doped GaN Treated with Low-Energy Electron Beam Irradiation (LEEBI)\n,” *Jpn. J. Appl. Phys.*, vol. 28, no. Part 2, No. 12, pp. L2112–L2114, 1989.

[28] S. Nakamura *et al.*, “High-Power GaN P-N Junction Blue-Light-Emitting Diodes,” *Jpn. J. Appl. Phys.*, vol. 30, pp. L1998, 1991.

[29] S. Nakamura, M. Senoh, N. Iwasa, and S. I. Nagahama, “High-brightness InGaN blue, green and yellow light-emitting diodes with quantum well structures,” *Jpn. J. Appl. Phys.*, vol. 34, no. 7, pp. L797–L799, 1995.

[30] 吉田 隆　編著:　次世代パワーデバイス半導体, 2009.

[31] W. Saito *et al.*, “Current Collapseless High-Voltage GaN-HEMT and its 50-W Boost Converter Operation,” in *2007 IEEE International Electron Devices Meeting*, 2007, pp. 869–872.

[32] R. Dwiliński *et al.*, “Bulk ammonothermal GaN,” *J. Cryst. Growth*, vol. 311, no. 10, pp. 3015–3018, 2009.

[33] F. Kawamura *et al.*, “Growth of GaN single crystals with extremely low dislocation density by two-step dislocation reduction,” *J. Cryst. Growth*, vol. 311, no. 10, pp. 3019–3024, 2009.

[34] I. C. Kizilyalli, A. P. Edwards, H. Nie, D. Bour, T. Prunty, and D. Disney, “3.7 kV vertical GaN PN diodes,” *IEEE Electron Device Lett.*, vol. 35, no. 2, pp. 247–249, 2014.

[35] T. Oka, Y. Ueno, T. Ina, and K. Hasegawa, “Vertical GaN-based trench metal oxide semiconductor field-effect transistors on a free-standing GaN substrate with blocking voltage of 1.6 kV,” *Appl. Phys. Express*, vol. 7, no. 2, 2014.

[36] G.B. Stringfellow, Organometallic vapor-phase epitaxy: theory and practice. 2nd Edition, 1999.

[37] I. C. Kizilyalli, A. P. Edwards, O. Aktas, T. Prunty, and D. Bour, “Vertical Power p-n Diodes Based on Bulk GaN,” vol. 62, no. 2, pp. 414–422, 2015.

[38] D. D. Koleske, A. E. Wickenden, R. L. Henry, and M. E. Twigg, “Influence of MOVPE growth conditions on carbon and silicon concentrations in GaN,” *J. Cryst. Growth*, vol. 242, no. 1–2, pp. 55–69, 2002.

[39] J. L. Lyons, A. Janotti, and C. G. Van de Walle, “Effects of carbon on the electrical and optical properties of InN, GaN, and AlN,” *Phys. Rev. B*, vol. 89, no. 3, p. 035204, 2014.

[40] T. Kachi, “Recent progress of GaN power devices for automotive applications,” *Jpn. J. Appl. Phys.*, vol. 53, no. 10, 2014.

[41] N. A. Fichtenbaum, T. E. Mates, S. Keller, S. P. DenBaars, and U. K. Mishra, “Impurity incorporation in heteroepitaxial N-face and Ga-face GaN films grown by metalorganic chemical vapor deposition,” *J. Cryst. Growth*, vol. 310, no. 6, pp. 1124–1131, 2008.

[42] J. L. Zhang, J. L. Liu, Y. Pu, W. Q. Fang, M. Zhang, and F. Y. Jiang, “Effects of carrier gas on carbon incorporation in GaN,” *Chinese Phys. Lett.*, vol. 31, no. 3, pp. 2011–2013, 2014.

[43] F. Kaess *et al.*, “Correlation between mobility collapse and carbon impurities in Si-doped GaN grown by low pressure metalorganic chemical vapor deposition,” *J. Appl. Phys.*, vol. 120, no. 10, 2016.

[44] W. V. Lundin *et al.*, “Study of GaN doping with carbon from propane in a wide range of MOVPE conditions,” *J. Cryst. Growth*, vol. 449, pp. 108–113, 2016.

[45] G. Piao *et al.*, “Study of carbon concentration in GaN grown by metalorganic chemical vapor deposition,” *J. Cryst. Growth*, vol. 456, pp. 137–139, 2016.

[46] T. Tanikawa, S. Kuboya, and T. Matsuoka, “Control of impurity concentration in N-polar ($000\bar{1}$) GaN grown by metalorganic vapor phase epitaxy,” *Phys. Status Solidi Basic Res.*, vol. 254, no. 8, pp. 1–5, 2017.

[47] Q. Mao *et al.*, “Influence of growth rate on the carbon contamination and luminescence of GaN grown on silicon,” *J. Semicond.*, vol. 36, no. 9, p. 093003, 2015.

[48] A. Ubukata, Y. Yano, H. Shimamura, A. Yamaguchi, T. Tabuchi, and K. Matsumoto, “High-growth-rate AlGaN buffer layers and atmospheric-pressure growth of low-carbon GaN for AlGaN/GaN HEMT on the 6-in.-diameter Si substrate metal-organic vapor phase epitaxy system,” *J. Cryst. Growth*, vol. 370, pp. 269–272, 2013.

[49] S. S. Liu and D. A. Stevenson, “Growth Kinetics and Catalytic Effects in the Vapor Phase Epitaxy of Gallium Nitride,” *J. Electrochem. Soc.*, vol. 125, no. 7, pp. 1161–1169, 1978.

[50] B. S. Sywe, J. R. Schlup, and J. H. Edgar, “Fourier transform infrared spectroscopic study of predeposition reactions in metalloorganic chemical vapor deposition of gallium nitride. 2,” *Chem. Mater.*, vol. 3, no. 6, pp. 1093–1097, 1991.

[51] D. Mazzarese, A. Tripathi, W. C. Conner, K. A. Jones, L. Calderon, and D. W. Eckart, “In situ FTIR and surface analysis of the reaction of trimethylgallium and ammonia,” *J. Electron. Mater.*, vol. 18, no. 3, pp. 369–377, 1989.

[52] J. R. Creighton and G. T. Wang, “Kinetics of metal organic-ammonia adduct decomposition: Implications for group-III nitride MOCVD,” *J. Phys. Chem. A*, vol. 109, no. 46, pp. 10554–10562, 2005.

[53] S. H. Kim, H. S. Kim, J. S. Hwang, J. G. Choi, and P. J. Chong, “In situ FTIR Analysis for the Thermal Decompositions of Trimethylgallium and Trimethylgallium-Ammonia Adduct,” *Chem. Mater.*, vol. 6, no. 3, pp. 278–281, 1994.

[54] J. Nishizawa, “On the Reaction Mechanism of GaAs MOCVD,” *J. Electrochem.*

Soc., vol. 130, no. 2, p. 413, 1983.

[55] M. J. Almond, C. E. Jenkins, D. A. Rice, and K. Hagen, “Organometallic precursors to the formation of GaN by MOCVD: structural characterisation of Me3Ga ?? NH3 by gas-phase electron diffraction,” *J. Organomet. Chem.*, vol. 439, no. 3, pp. 251–261, 1992.

[56] J. Schäfer, A. Simons, J. Wolfrum, and R. A. Fischer, “Detection of gas-phase species in MOCVD of GaN using molecular beam quadrupole mass spectrometry,” *Chem. Phys. Lett.*, vol. 319, no. 5–6, pp. 477–481, 2000.

[57] A. Thon and T. F. Kuech, “High temperature adduct formation of trimethylgallium and ammonia,” *Appl. Phys. Lett.*, vol. 69, no. 1, pp. 55–57, Jul. 1996.

[58] M. Yoshida and H. Wantanabe, “Mass Spectrometric Study of Ga(CH3)3 and Ga(C2H5)3 Decomposition Reaction in H2 and N2,” *J. Electrochem. Soc. Solid-State Sci. Technol.*, vol. 132, no. 3, pp. 677–679, 1985.

[59] O. Ambacher *et al.*, “Thermal stability and desorption of group III nitrides prepared by metal organic chemical vapor deposition,” *J. Vac. Sci. Technol. B Microelectron. Nanom. Struct.*, vol. 14, no. 6, pp. 3532–3542, 1996.

Chapter 2 Experimental equipment and preliminary results

2.1 Introduction

In this chapter, the MOVPE system used for the preliminary measurement of gas phase reaction in this study is first introduced. A TOF-MS system (infiTOF-UHV, MSI.TOKYO, Inc.) employed in our study has a high resolution of beyond 0.002 u. By using the experimental setup of the MOVPE reactor coupled to the TOF gas monitoring system, we tried to measure the reaction inside the reactor. Some preliminary results will be shown in this chapter. In order to make experiments more convenient, we have designed a simple reactor which also will be introduced.

2.2 MOVPE system

Figure 2-1 shows a schematic diagram of the MOVPE system. The MOVPE system is a pressurized MOVPE manufactured by EpiQuest. (Nagoya University Amano Laboratory MOVPE No. 5) All raw materials and carrier gas are supplied to the reaction furnace with their flow rates controlled by a mass flow controller (MFC). Liquid organo-metallic TMGa is a gas-phase raw material supply that is saturated by bubbling with H_2 gas. The temperature of TMGa was kept at 5 ° C using a constant temperature because it was greatly changed by the surrounding temperature. Further, in order to prevent the solidification of the raw material in the raw material supply line, the pipe temperature was set to 55 ° C. using a tape heater. The growth pressure was determined by the total

gas flow rate and the pumping speed of the dry pump (DRP). In the temperature control, the temperature is measured by a thermocouple near the heater, and the temperature is controlled by a temperature controller. The difference between the heater temperature and the substrate temperature is about 100 ° C.

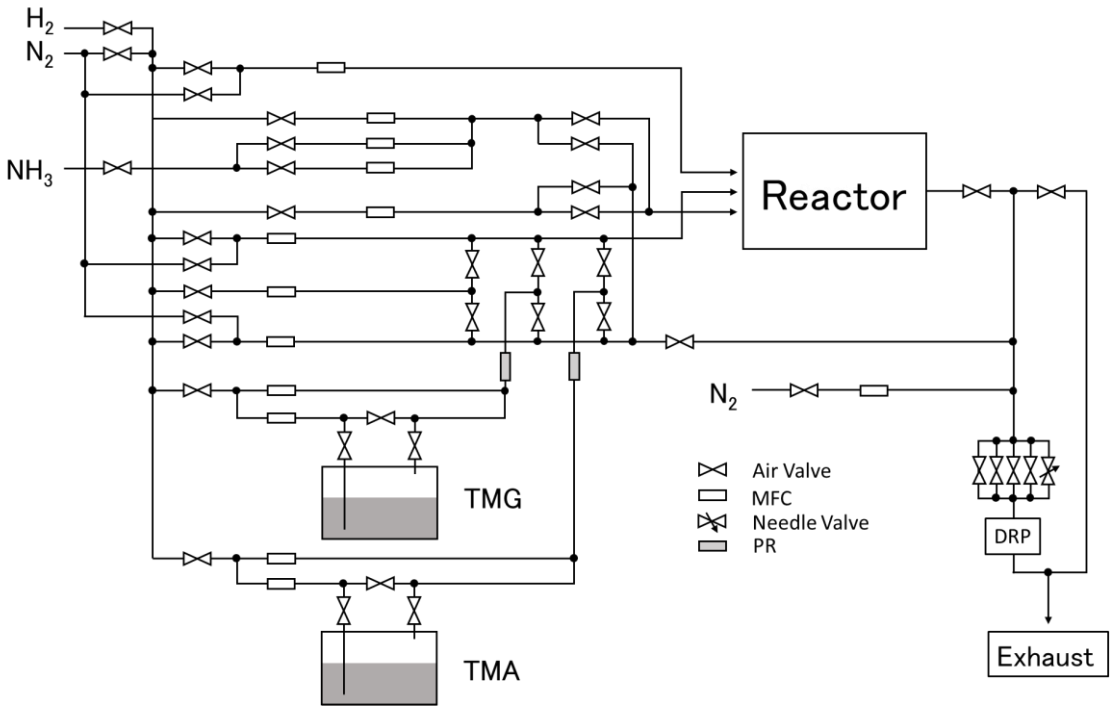

Figure 2.1 Schematic diagram of the MOVPE system

2.3 TOF-MS system

The TOF-MS system used in this study has a multi flight method. This method makes it possible to fly the ion around the desired number of times to realize a long flight path and its associated high accuracy in a small set-up. The measurement has a linear mode

and a multi-mode. A schematic diagram of each is shown in Figure 2.2. The linear mode has a flight path that passes through the detector without orbiting. In this measurement, a wide m / z range can be observed at a time. However, the m / z measurement accuracy is inferior to the multi-mode. As described at the beginning of the section, the multi-mode has a flight path in which the figure-shaped flight path orbits an arbitrary number of times and passes through a detector. This measurement observes a narrow m / z range specified by the user.

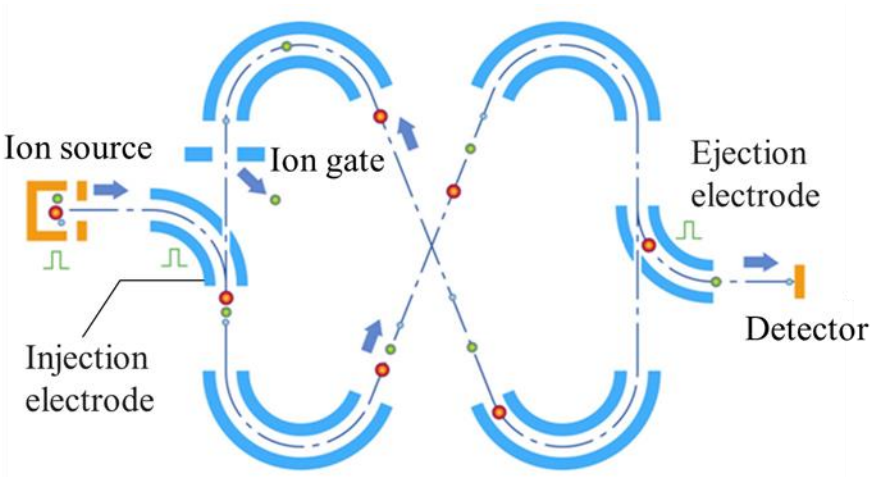

Figure 2.2 Multiple turn mass analyzer [8]

2.4 Preliminary results

In order to determine the reliability of TOF-MS, we tested it with an TMGa cylinder which only few MO inside and compared the test results of a conventional QMS. The

comparison results are shown in Figure 2.3. Both mass spectrometers show corresponding peaks in almost the same places, which illustrates the authenticity of the data. Obviously, through the detection of the ToF-MS system, the same mass number molecules are clearly distinguished. The data results show the high-resolution characteristics of TOF-MS.

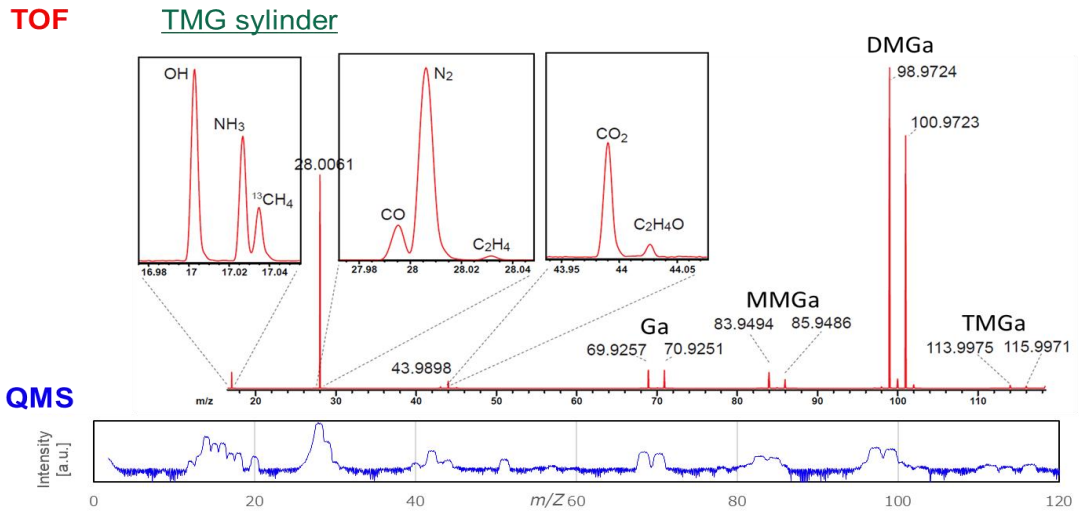

Figure 2.3 TMGa cylinder results for TOF-MS and QMS mass spectrometry

After determining the reliability of the device, we entered the actual measurement phase of the MOVPE system. Figure 2.4 shows the experimental setup of the MOVPE reactor coupled to the TOF gas monitoring system. In this system, two gas sampling lines were affixed on the reactor, and an in situ monitoring line was installed at the center of the wafer's upper surface. The microtube for the other line was aligned with the exhaust line just behind the reactor. The size of the quartz flow channel in the reactor was designed

according to a single 4-inch wafer. The microtube length and diameter were 50 and 100mm, respectively, and out-of-reactor region was heated at 120 ℃.

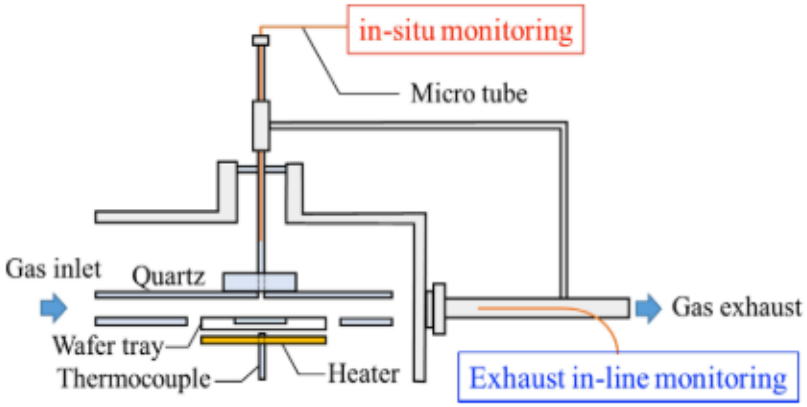

Figure 2.4 Schematic diagram of the metalorganic vapor-phase epitaxy reactor and mass spectrometry microtubes [9].

To set the ionization energy for the monitoring detector, the decomposition of TMGa in the in situ monitoring line was measured at a room temperature [9]. Figure 2.5 shows the intensity plots of the observed TMGa, dimethylgallium (DMGa), monomethylgallium (MMGa), Ga, and methane signals. The intensity of each species became stable at ionization energy of 14eV, which was chosen for this analysis. From the spectral intensities and for the convenience of the analysis, both methane and DMGa were considered as proofs of the TMGa reaction process. The behavior at ionization dependence has matched with the previous study [1].

Partial pressures of respective precursor flows were maintained similar to a conventional MOVPE of GaN (10 um/h for the drift layer of the power device). The TMGa flow rate was 430 μmol/min, and the V/III ratio was 230 under in the presence of ammonia. During the 1-h monitoring period, the temperature increased gradually from the room temperature to 1100 ℃. The surface temperature of the susceptor was measured by fixing a thermocouple at the susceptor surface. The reactor pressure was 200 Torr, and the flow speed in the reactor was 1.5 m/s.

Figure 2.6(a) shows the mass spectrum of the in situ monitoring at m/z = 16 at a room temperature. NH_2 is a typical fragment of ammonia and yields a strong signal under conventional growth conditions. The NH_2 and CH_4 signals were clearly separated although both the compounds had similar masses. Moreover, their peak values precisely matched the theoretical mass values. This indicated the availability of observing CH_4 signals in the presence of ammonia. Figure 2.6(b) shows the peaks of the DMG isotopes. The mass positions and intensity ratios of these peaks also precisely matched their theoretical values, confirming that this system can completely specify the reactants in the complex reactions of actual MOVPE systems.

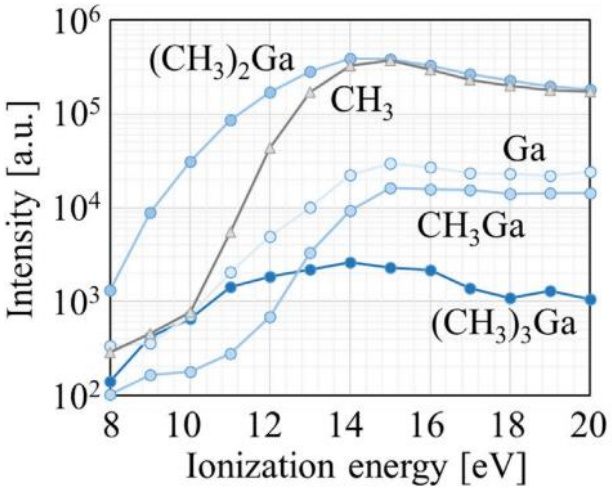

Figure 2.5 Ionization energy of mass spectrometry in trimethyl- gallium flow at a room

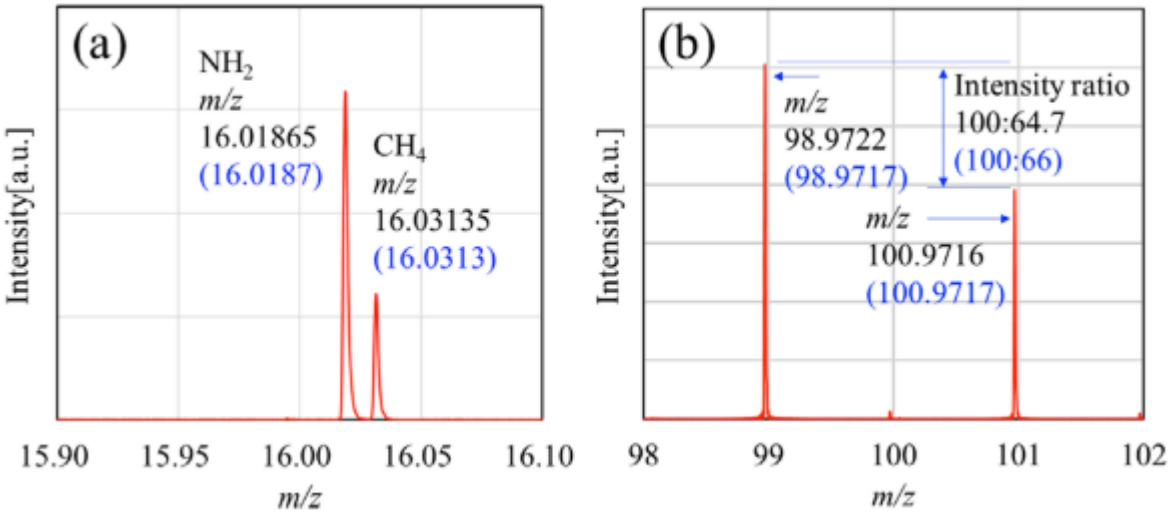

Figure 2.6 Mass spectrum obtained during in situ monitoring. (a) NH_2 and CH_4 peaks around 16 m/z and (b) dimethylgallium (DMG) isotope peaks around 100 m/z (theoretical masses are given in parentheses).

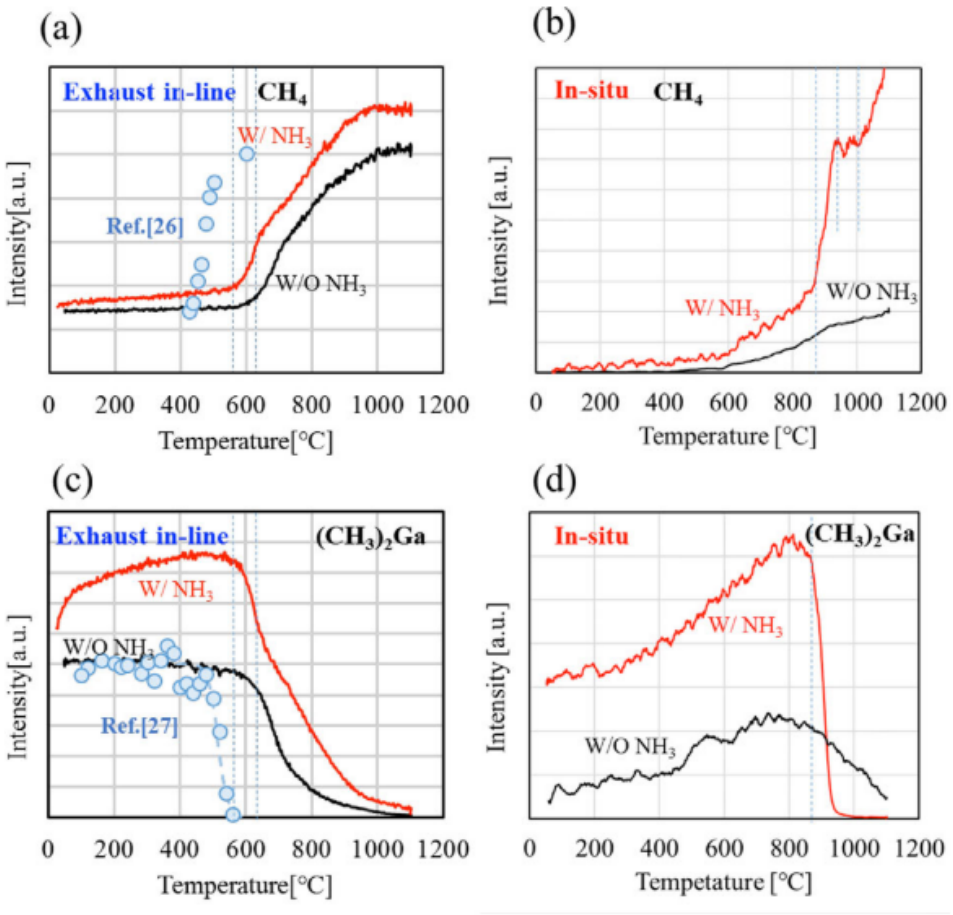

Figure 2.7 Temperature dependence of methane and DMG signals (with and without ammonia flow). (a) Exhaust in-line monitoring and (b) in-line monitoring of CH4 signals. (c) Exhaust in-line monitoring and (d) in-line monitoring of DMG signals (red line: with ammonia; black line: without ammonia). For comparison, the data on DMG and methane from literature were included with the exhaust data from Larsen et al. [7] (shifted by 80℃) and Bahlawane et al. [8].

Figure 2.7 plots the temperature dependence of the methane and DMG signal intensities in the presence and absence of the ammonia supply [9]. When the temperature in the exhaust line reaches 550 ℃, the TMGa starts to decompose. Consequently, the DMG signal flow decreases (Fig. 2.7c), whereas the methane signal flow increases (Fig. 2.7a). The change of the methane and DMG signals followed previous literature data, confirming the present setup. The presence of ammonia slightly decreased the decomposition temperature of TMGa, as reported in the previous studies [1-3]. Panels (b) and (d) show the methane and DMG signal intensities, measured at the in situ line monitoring port. As the gas-phase temperatures at this port were lower (the so-called "cold finger"), there is allows for estimating even intermediate products that are a temperature offset of 250 ℃ to the exhaust line. This then fully reacted at the exhaust port.

At both the sampling points, the change is similar. One can observe two distinct plateaus in the DMG and even more clearly in the methane signal. At temperatures >700 ℃ (or 950 ℃at in situ port), the slope of the DMG signal changes. At 900 ℃, the second plateau was reached. Within this temperature range, MMG appeared to be stable and dominant. The CH_4 intensity rapidly increased above 1000 ℃, reflecting the MMG decomposition due to the presence of active hydrogen resulting from NH3 decomposition [4]. Without the active hydrogen from ammonia, the colder gas-phase temperatures at the

in-situ port were not sufficient for complete decomposition of the DMG; it remained stable even at 1100 ℃.

The result confirmed the following reactions:

$(CH_3)_3Ga \rightarrow (CH_3)_3Ga + CH_3$ (2.1)

$(CH_3)_2Ga \rightarrow (CH_3)Ga + CH_3$ (2.2)

$(CH_3)_3Ga + *NH_3 \rightarrow Ga + CH_4 + NH_2$ (2.3)

As mentioned in the last reaction, the hydrogen was obtained from the activated NHx, which is in agreement with the earlier works using AsD_3 [5]. The reason is a very high activation energy when the last CH_3 group was removed. The other decomposition steps could also occur via the formation of C_2H_6 by the attack of CH_3 radicals, although literature suggests that this is an unfavorable pathway. Instead, the active methyl groups from step (1) or (2) could attack NH_3 and form an adduct as suggested by Jacko and Prices [6].

Therefore, the traces of the adducts were searched for such product. Figure 2.8 shows the temperature dependence of the signals of $(CH_3)_2Ga$ and its adduct with NH_3 ($(CH_3)_2Ga$: NH_3), measured at the in situ monitoring port in the presence of ammonia. The experiment and monitoring for adduct monitoring were the same condition at Fig. 2.7(d) except integration times. There is a clear signal, although the intensity was 1000 times smaller. Thus, the adduct pathway was not very likely. Furthermore, the $(CH_3)_2Ga$

and its adduct decomposed in a similar manner, because the DMG and the adduct signal reduce at similar temperatures. The adduct formation favored a decomposition by active hydrogen, which was further confirmed by peaks in the mass spectrum which would correspond to hydrogenated TMGa, such as $(CH_3)_2GaHx$. However, further studies are required to identify more adducts

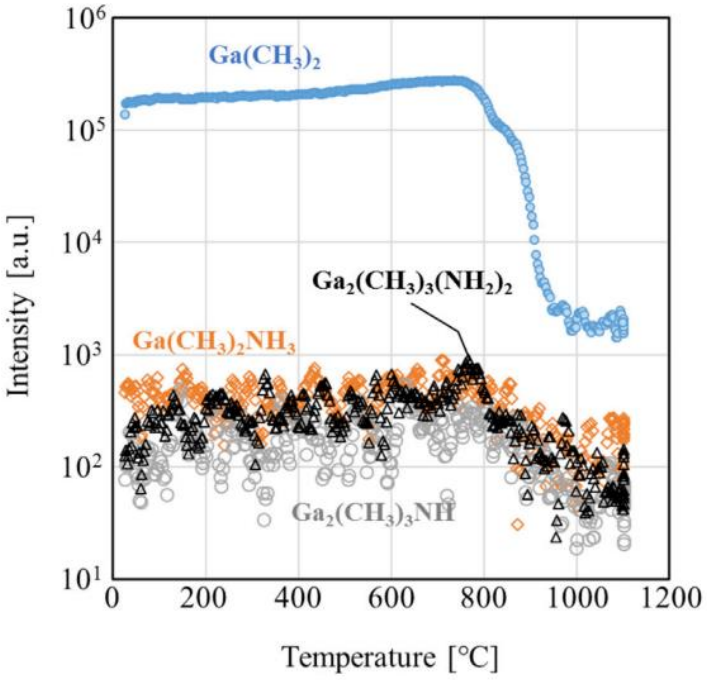

Figure 2.8 Temperature dependences of DMG (blue circles) and DMG:NH_3 adduct (black, orange, and grey symbols) signal intensities in the presence of ammonia [9].

Thus, the adduct pathway was not very likely. Furthermore, the $(CH_3)_2Ga$ and its adduct decomposed in a similar manner, because the DMG and the adduct signal reduce

at similar temperatures. The adduct formation favored a decomposition by active hydrogen, which was further confirmed by peaks in the mass spectrum which would correspond to hydrogenated TMGa, such as $(CH_3)_2GaHx$. However, further studies are required to identify more adducts and their ratio.

2.5 A sample reactor

The above results reveal the feasibility of TOF-MS for MOVPE gas phase reaction analysis. In order to perform gas phase reaction analysis more conveniently. we have designed a simple reactor. All subsequent experiments were performed in the simple reactor formed by an external heated quartz tube (diameter: 30 mm, heated length: 30 cm), as shown in Fig. 2.8. The photograph of the sample reactor was shown in Fig.2.9. The gas was sampled via another quartz glass tube introduced from the back of the reactor. The entry position of the sampling gas tube could be varied during heating. A 0.1 mm fused silica capillary connected the gas tube to the entry of the TOF-MS system. All gas

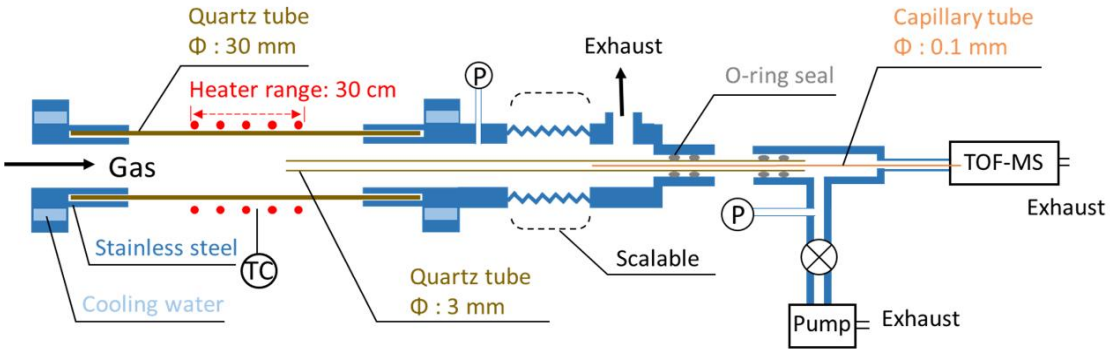

Fig. 2.8 Schematic of the monitoring system.

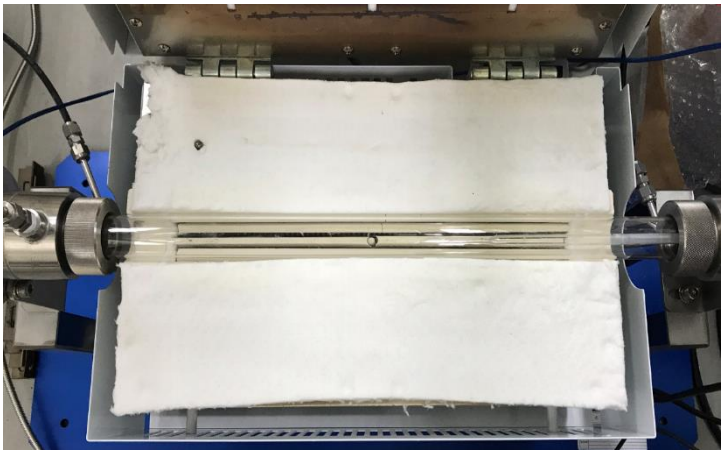

Fig. 2.9 the photograph of the sample reactor.

lines were heated at 80°C to prevent gases (especially water) from adhering to the surfaces.

At high flow rates, the actual reaction in the MOVPE reactors is typically in a non-equilibrium state with local heating. Decreasing the reaction time at high flow rates will reduce the reaction rate in the gas phase, which hinders the reaction monitoring. This study focuses on the reaction process in the near-equilibrium state. Therefore, the experiments were conducted at a low flow rate (1 l/min), which resulted in a flow speed of about 0.03 m/s at RT. The large differences in heat capacity and thermal conductivity between H_2 and N_2 cause the actual gas phase temperatures in the reactor to significantly deviate from the wall temperature. To obtain the actual temperature distribution inside the reactor, the temperature was measured at the center of the reactor tube using a thermocouple inside a thin quartz tube with a sealed apex. Figure 2.10 shows the

measured temperature distributions under H_2 and N_2 atmospheres at a heater temperature. Each heat distribution shows a broad maximum between 15 and 20 cm at about 50°C below the heater setpoint at 1000 ℃. Thus, all temperatures in the experiment were corrected to the measured gas phase temperatures.

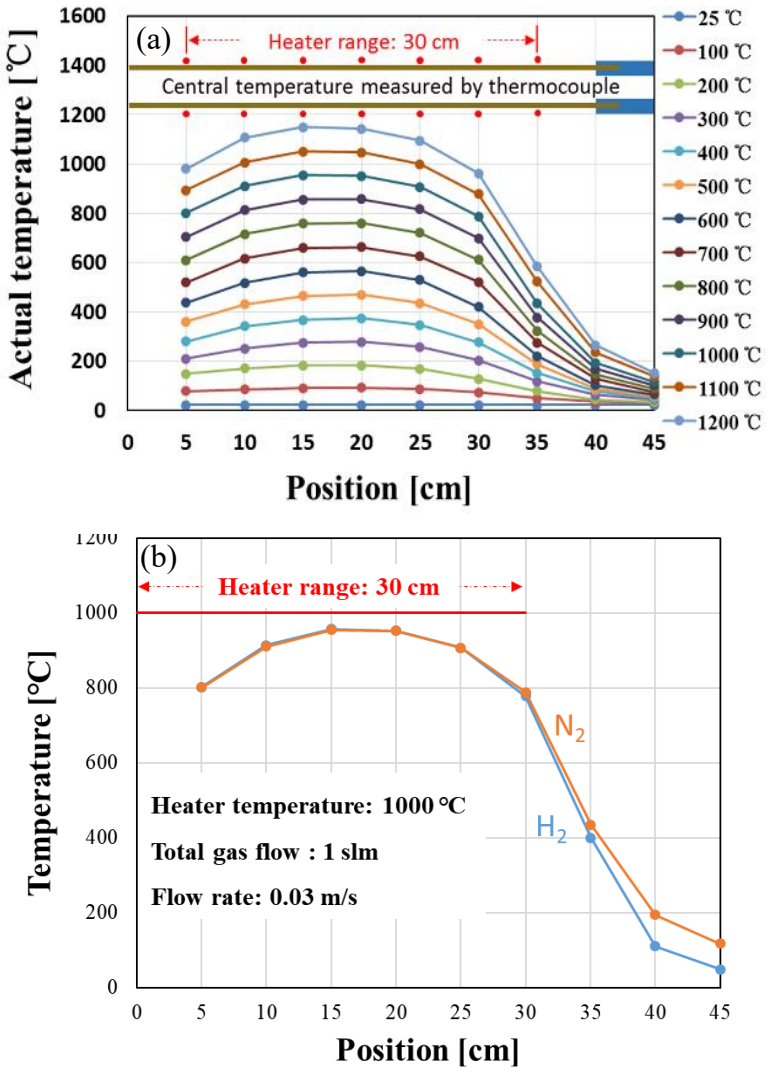

Fig. 2.10 (a) Actual temperature distribution in the reactor at various heater temperatures in N_2 atmosphere, and (b) Actual temperature distribution in different carrier gas atmospheres at a heater temperature of 1000 ℃.

2.6 Summary

In this chapter, our experimental equipment and related preliminary data are introduced in detail. The reliability of the mass spectrometer was tested. ToF-MS proved to be suitable for the analysis of complicated MOVPE gas-phase reactions through the detection results of a conventional quadrupole mass spectroscopy (QMS) and the actual observation experiments introduced into the actual reactor. In situ monitoring of TMGa decomposition and its adduct formation with NHx at a very wide range of temperatures and a very high signal- to-noise ratio were demonstrated by using a high-resolution and high-sensitivity TOF mass spectrometry in a commercial MOVPE reactor. Due to the inconvenient control of the temperature distribution and other conditions in the real reactor, in order to conduct experiments more conveniently, we have designed a simple reactor. By measuring the thermocouple and controlling the flow rate, the same heat distribution in different carrier gases is achieved. Further accurate measurements become possible.

2.7 References

[1] U. Bergmann, V. Reimer, and B. Atakan, “Gas phase studies of trimethylgallium with ammonia, propylamine and water at elevated temperatures: Towards an understanding of GaN growth and oxygen incorporation,” *Phys. Status Solidi Appl. Res.*, vol. 176, no. 1, pp. 719–722, 1999.

[2] A. Thon and T. F. Kuech, “High temperature adduct formation of trimethylgallium and ammonia,” *Appl. Phys. Lett.*, vol. 69, no. 1, pp. 55–57, Jul. 1996.

[3] M. Yoshida and H. Wantanabe, “Mass Spectrometric Study of Ga(CH3)3 and Ga(C2H5)3 Decomposition Reaction in H2 and N2,” *J. Electrochem. Soc. Solid-State Sci. Technol.*, vol. 132, no. 3, pp. 677–679, 1985.

[4] S. S. Liu and D. A. Stevenson, “Growth Kinetics and Catalytic Effects in the Vapor Phase Epitaxy of Gallium Nitride,” *J. Electrochem. Soc.*, vol. 125, no. 7, pp. 1161–1169, 1978.

[5] C. A. Larsen, N. I. Buchan, and G. B. Stringfellow, “Reaction mechanisms in the organometallic vapor phase epitaxial growth of GaAs,” *Appl. Phys. Lett.*, vol. 52, no. 6, pp. 480–482, 1988.

[6] M. G. Jacko and S. J. W. Price, “The pyrolysis of trimethyl gallium,” *Can. J. Chem.*, vol. 41, no. 6, pp. 1560–1567, 1963.

[7] N. BAHLAWANE, F. REILMANN, L. SALAMEH, and K. KOHSEHOINGHAUS, “Mass-Spectrometric Monitoring of the Thermally Induced Decomposition of Trimethylgallium, Tris(tert-Butyl)Gallium, and Triethylantimony at Low Pressure Conditions,” *J. Am. Soc. Mass Spectrom.*, vol. 19, no. 7, pp. 947–954, Jul. 2008.

[8] http://www.kanomax.co.jp/product/index_0116.html

[9] K. Nagamatsu, S. Nitta, Z. Ye, H. Nagao, S. Miki, Y. Honda, and H. Amano, "Decomposition of trimethylgallium and adduct formation in a metalorganic vapor phase epitaxy reactor analyzed by high-resolution gas monitoring system," *Phys. status solidi*, vol. 254, no. 8, p. 1600737, Aug. 2017.

Chapter 3 Ammonia Decomposition and Reaction

3.1 Background

Most of the fundamental MOVPE investigations were carried out in the 80's, when III-nitrides were not widely studied. Hence, many investigations on the decomposition of trimethylgallium (TMGa) exist [1], but very few works have been published on ammonia (NH3) decomposition. The earliest study was on chloride vapor phase epitaxy (Cl-VPE) reactors using mass spectrometry [5] or even titration [6] to determine the amount of NH3 remaining in the exhaust of reactors. In these studies, low NH3 decomposition ratios of only a few percent were found even at 1000°C and above. Thermodynamic analysis in equilibrium showed that NH_3 decomposes almost completely into inert nitrogen and hydrogen at about 400°C [2]. This stark difference in decomposition is due to the very low conversion ratio of NH_3 in the absence of catalysts [8, 3]. At 800°C, it takes more than 30 min to observe some decomposition [3], whereas at 1000°C just 2 min is needed [4]. However, the typical flow speed of up to a few meters per second in MOVPE corresponds to gas residence times in the hot zone on the order of seconds rather than minutes. Moreover, the decomposition of NH_3 has only been studied in the cases of VPE [5, 6] and for the conversion of NH_3 to hydrogen (H_2) as a fuel [8]. The only study involving TMGa did not report on NH_3 decomposition [7]. For understanding the vapor

phase growth process of group-III nitrides, the decomposition of NH_3 will be discussed at various sampling locations inside the reactor over a wide range of temperatures. The activation energy of the decomposition of NH_3 is also obtained based on the measured results assuming a first-order reaction.

3.2 Experiments

As stated in the previous chapter, this experiment was performed on a simple reactor. The total gas flow was 1 slm and the NH_3 gas flow was 50 sccm. The resulting flow speed was 0.02 m/s at room temperature (RT), corresponding to a residence time inside the heated zone of about 15 s.

Figure 3.1(a) shows the mass spectrum recorded around m/z = 18 at RT, in which the species of H_2O, $^{15}NH_3$, and NH_4 were clearly distinguished. Thus, the resolution of our system is sufficient to investigate the mechanism of the vapor phase growth of III-nitrides.

Great care was taken to avoid the presence of any metals in the sampling gas path because the NH_3 decomposition ratio can be strongly enhanced by various metals such as tungsten (W) [4, 9], molybdenum (Mo) [11], platinum (Pt) [12, 13], and iron (Fe) [14-16]. Furthermore, in our first test, the gas was sampled at the stainless-steel exhaust of the MOVPE reactor [10], and then a rather high ratio of NH_3 decomposition was observed.

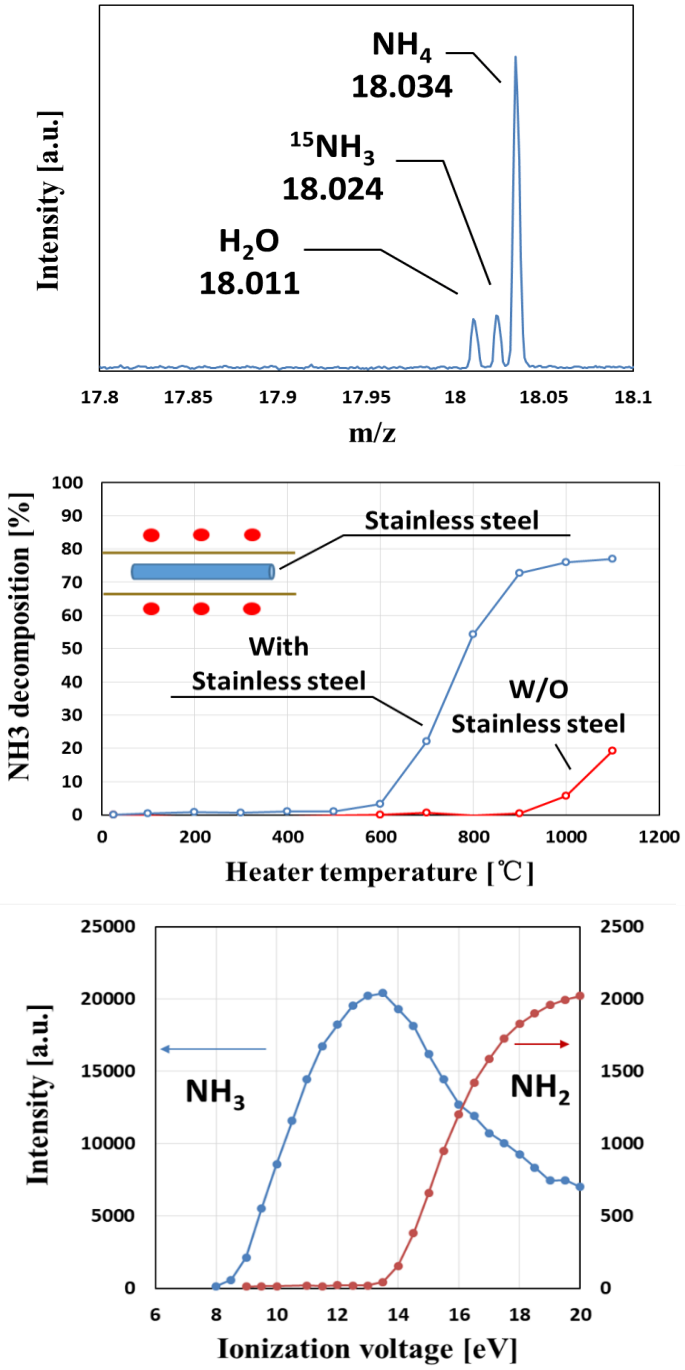

Fig. 3.1 (a) Mass spectrum recorded around m/z (mass-to-charge ratio) =18; (b) NH_3 decomposition in the stainless steel and quartz reactors; and (c) dependence of NH_3 and $\cdot NH_2$ intensities on ionization voltage.

This result was reproduced by our simple reactor: when a piece of stainless steel was placed in the reactor at a heater temperature of 800 °C, then the decomposition exceeded 50 %, whereas it was almost zero without the steel (Fig. 3.1(b)).

NH_3 may also decompose during the ionization at the entry of the TOF-MS system. The fragmentation due to ionization should change the obtained decomposition ratio, especially when temperature-dependent measurements are performed. Thus, we first measured the impact of the ionization at RT on the signals of NH_3 and NH_2. The latter is a typical fragment of NH_3 and yields a strong signal. Figure 3.1(c) shows that the fragmentation of NH_3 occurred when the ionization voltage was 14 eV and above. Therefore, an ionization voltage of 12 eV was chosen for our experiment.

3.3 Results and discussion

The temperature distribution of the actual gas is required to analyze the reaction. Therefore, we measured the temperature in the center of the reactor tube with a thermocouple in N_2 atmosphere as shown in Fig. 2.10(a). It can be seen that even though the heater was 30 cm long, the temperature had already started to drop by 25 cm. Furthermore, the maximum temperature is also slightly offset, which is likely caused by the heat transport along the quartz tube. The temperature between 15 and 20 cm was nearly constant, hence this can be defined as the gas phase temperature.

For the measurement of NH_3 decomposition, gas was sampled in the reactor between the inlet and the outlet at intervals of 5 cm. At each position, the heater temperature of the reactor was increased from RT to 1200°C. We then calculated the NH_3 decomposition

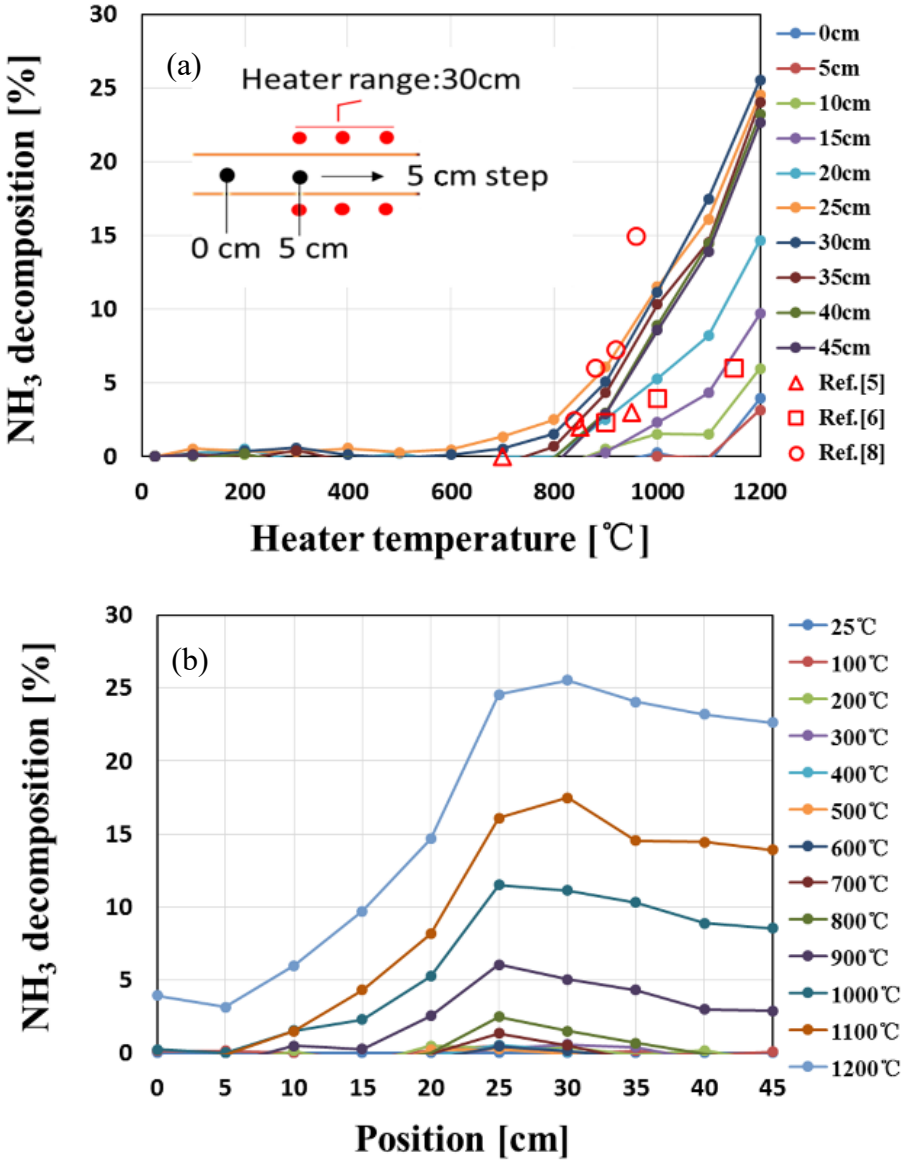

Fig. 3.2 (a) Measured NH_3 decomposition with varying temperature at different sampling positions together with literature data (Δ [5], □ [6], ○ [8]) and (b) NH_3 decomposition at each sampling position for different heater temperatures.

ratio from the peak intensity at different temperatures.

Figure 3.2(a) shows the temperature dependence of the NH_3 decomposition at each sampling position, referenced with data from the literature. The onset of NH_3 decomposition is at approximately 700°C. The decomposition increases with increasing temperature. However, at 1200°C the maximum decomposition ratio is only 25.5% (30 cm from the inlet). Our data at this position are consistent with previous research results from Cooper and Ljungström [8]. The earlier data of Ban [5] and Liu and Stevenson [6], obtained by mass spectrometry and titration, better follow our data closer to the inlet at 15 cm. Therefore, their reported lower decomposition ratio is likely due to the shorter residence time of the NH_3 in the hot zone of their reactors, either because of a smaller hot zone or because of a higher flow speed. This suggests that the residence time is an important factor. If the residence time in the hot zone is known, then the NH_3 decomposition can be scaled between different reactors.

Figure 3.2(b) shows the position dependence of the NH_3 decomposition. After an initial rapid increase, a slight reduction of the decomposition ratio was observed beyond 30 cm towards the end of the reactor. This could be explained by the pressure change due to heating, which might have affected thermal diffusion of molecules with a different mass in the capillary, or simply by further decomposition in the sampling capillary, which was more intensely heated when placed deeper in the hot zone. The exact cause of the observed reduction is currently under further investigation.

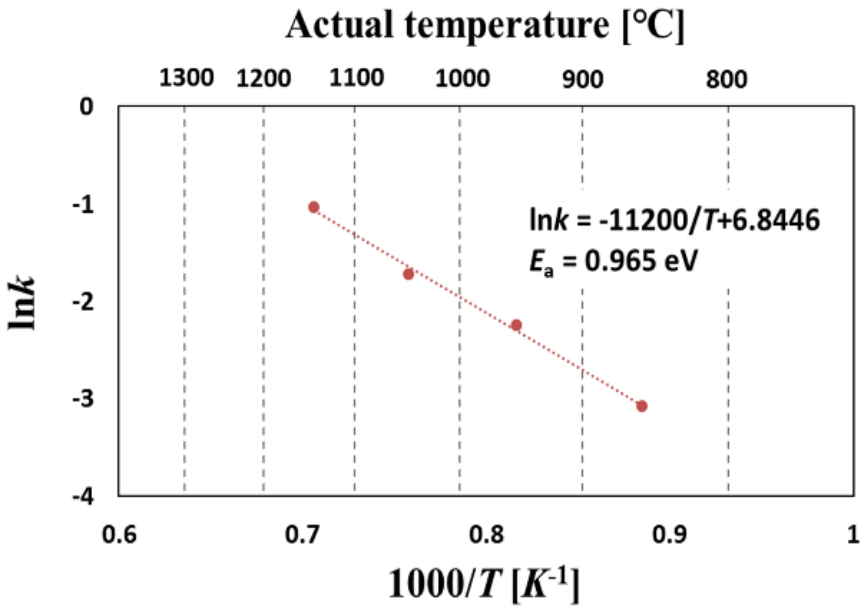

Fig. 3.4 Arrhenius plot of the reaction rate for NH_3 decomposition.

Since the decomposition strongly depends on temperature, to calculate decomposition ratios, we need the residence time at high temperatures. According to Fig. 2.10, the temperature distribution in the reactor is relatively stable between 15 and 20 cm. I followed the procedure of Cooper and Ljungström [8] to estimate the reaction rate assuming a first-order reaction. The reaction rate k is then given by the change in concentration with respect to the residence time, $k[NH_3] = -d[NH_3]/dt$, where $[NH_3]$ is the NH_3 concentration at reaction time t. The reaction time was assumed to be the time it takes for the gas to flow the 5 cm between 15 and 20 cm, and the NH_3 concentration ratio was obtained from the change in the NH_3 peak intensity between 15 and 20 cm.

The obtained *k* was plotted as a function of the inverse of temperature to estimate the activation energy (Fig. 3.4). The activation energy is estimated to be 0.965 ± 0.004 eV. This is much lower than the value of 4.6 ± 0.2 eV for NH_3 decomposition in quartz bulbs obtained by Hinshelwood and Burk [4] and also lower than the value of 1.5 eV obtained by Cooper and Ljungström [8] which was estimated from a similar calculation. The only other comparably low activation energy has been a value of 0.76 eV reported for Pt-catalyst-assisted NH_3 decomposition [17]. As previously shown in Fig. 3.1(c), a high ionization voltage causes the fragmentation of NH_3. On the other hand, N_2 and H_2 are very stable and difficult to ionize at low voltages. Since Cooper and Ljungström [8] also monitored N_2 and H_2 signals, their estimation may have been influenced by the fragmentation of NH_3 due to ionization. Furthermore, our data are derived from the vanishing of the NH_3 signal, i.e., the first step of $NH_3 \rightarrow NH_2$, which might have a lower activation energy than the following steps. This may also explain the much higher values obtained by Hirnshelwood and Burk [4]. Moreover, the in situ data reported by Liu and Stevenson [6] were measured by chemical titration of the remaining NH_3, and their temperature dependence is in good agreement with our data for the vanishing of the NH_3 signal. I therefore have evidence that the ionization is not the cause of the deviation from our data.

3.4 Summary

The decomposition of NH_3 at various sampling locations over a wide range of temperatures in a simple reactor was systematically measured using a high-resolution TOF-MS system. Great care was taken to avoid any metal in the sampling gas path since this would have greatly increased decomposition, i.e., by shifting the onset of decomposition from 950 to 700°C. Our data reproduced previous results with differences apparently caused by different gas residence times in the hot zones. From our temperature profiles we estimated the residence time in the hot zone and calculated the reaction rates. The obtained temperature dependence gave a low activation energy of 0.965 $\pm$ 0.004 eV.

3.5 References

[1] G.B. Stringfellow, Organometallic vapor-phase epitaxy: theory and practice. 2nd Edition, 1999.

[2] B. Beaumont *et al.*, "Nitrogen precursors in metalorganic vapor phase epitaxy of (A1,Ga)N," *Growth (Lakeland)*, vol. 156, pp. 140–146, 1995.

[3] D. Dirtu, L. Odochian, A. Pui, and I. Humelnicu, "Thermal decomposition of ammonia. N2H4- An intermediate reaction product," *Cent. Eur. J. Chem.*, vol. 4, no. 4, pp. 666–673, 2006.

[4] J. Chapman, J. Hinshelwood, and J. Prichard, "123, 2730), and nitrous oxide (Hinshelwood and Burk," 1899.

[5] V. S. Ban *et al.*, "Mass Spectrometric Studies of Vapor-Phase Crystal Growth," *J. Electrochem. Soc.*, vol. 119, no. 6, p. 761, 1972.

[6] S. S. Liu and D. A. Stevenson, "Growth Kinetics and Catalytic Effects in the Vapor Phase Epitaxy of Gallium Nitride," *J. Electrochem. Soc.*, vol. 125, no. 7, pp. 1161–1169, 1978.

[7] J. Schäfer, A. Simons, J. Wolfrum, and R. A. Fischer, "Detection of gas-phase species in MOCVD of GaN using molecular beam quadrupole mass spectrometry," *Chem. Phys. Lett.*, vol. 319, no. 5–6, pp. 477–481, 2000.

[8] D. A. Cooper and E. B. Ljungström, "Decomposition of NH3 over Quartz Sand at 840-960 ºC," *Energy & Fuels*, vol. 2, no. 8, pp. 716–719, 1988.

[9] H. Shindo, C. Egawa, T. Onishi, and K. Tamaru, "Reaction mechanism of ammonia decomposition on tungsten," *J. Chem. Soc. Faraday Trans. 1 Phys. Chem. Condens. Phases*, vol. 76, pp. 280–290, 1980.

[10] K. Nagamatsu *et al.*, "Decomposition of trimethylgallium and adduct formation in a metalorganic vapor phase epitaxy reactor analyzed by high-resolution gas monitoring system," *Phys. Status Solidi Basic Res.*, vol. 254, no. 8, pp. 1–4, 2017.

[11] R. E. Burk, "The Thermal Decomposition of Ammonia upon the Surface of a Molybdenum Wire," *Proc. Natl. Acad. Sci.*, vol. 13, no. 2, pp. 67–74, Feb. 1927.

[12] S. Kenichi, D. Hironaga, A. Mihara, A. Hashimoto, and A. Yamamoto, “Catalyst Temperature Dependence of NH 3 Decomposition for InN Grown by Metal Organic Vapor Phase Epitaxy,” *Jpn. J. Appl. Phys.*, vol. 52, no. 08, p. 08JD04, 2013.

[13] S. F. Yin, Q. H. Zhang, B. Q. Xu, W. X. Zhu, C. F. Ng, and C. T. Au, “Investigation on the catalysis of COx-free hydrogen generation from ammonia,” *J. Catal.*, vol. 224, no. 2, pp. 384–396, 2004.

[14] W. Arabczyk and J. Zamlynny, “Study of the ammonia decomposition over iron catalysts,” *Catal. Letters*, vol. 60, pp. 167–171, 1999.

[15] W. Arabczyk and U. Narkiewicz, “A new method for in situ determination of number of active sites in iron catalysts for ammonia synthesis and decomposition,” *Appl. Surf. Sci.*, vol. 196, no. 1–4, pp. 423–428, 2002.

[16] G. Ertl and M. Huber, “Mechanism and kinetics of ammonia decomposition on iron,” *J. Catal.*, vol. 61, no. 2, pp. 537–539, 1980.

[17] S. Kenichi, D. Hironaga, A. Mihara, A. Hashimoto, and A. Yamamoto, “Catalyst Temperature Dependence of NH 3 Decomposition for InN Grown by Metal Organic Vapor Phase Epitaxy,” *Jpn. J. Appl. Phys.*, vol. 52, no. 08, p. 08JD04, 2013.

Chapter 4 Analysis of Trimethylgallium Decomposition

4.1 Background

The overall reaction process in MOVPE can be divided into two parts, a gas phase reaction and a surface reaction [2]. The raw materials transported to the heating zone by the carrier gas react in the gas phase and finally crystallize on the surface of the substrate. The analysis of the gas phase reaction is crucial to the clarification of the overall reaction and the realization of theoretical calculations [3]. Trimethylgallium ($Ga(CH_3)_3$) is commonly used as the gallium (Ga) precursor. Hence, a clear understanding of $Ga(CH_3)_3$ thermal decomposition process in gas phase is necessary. Most decomposition studies of $Ga(CH_3)_3$ were completed in the 1980s [4 – 9]. However, because of their aim of growing GaAs, these studies focused on the temperature range of 300 – 700 °C which is considerably below the growth temperature of GaN of about 1000-1100 °C. Therefore, the decomposition reaction of $Ga(CH_3)_3$ at high temperatures of about 1000 ℃ needs to be revisited.

In this study, we investigated the decomposition of $Ga(CH_3)_3$ in different carrier gases (H_2 and N_2) at temperatures ranging from room temperature (RT) to 1200 ℃.

4.2 Experimental details

The pressure inside the reactor was set to 99 kPa (almost atmospheric pressure). The internal pressure of the thin quartz tube was 30 kPa lower than the pressure of the reactor to ensure the rapid transport of gases to the TOF-MS system.

Because of the large differences in heat capacity and thermal conductivity between H_2 and N_2, the actual gas phase temperatures in the reactor can deviate considerately from the wall temperature. Therefore, we conducted the experiments at a low flow rate of 1 l/min, which resulted in a flow speed of about 0.03 m/s at RT, just same as previous e xperimental conditions. The measured temperature distributions at a heater temperature 1000℃ of H_2 and N_2 atmospheres as shown in Fig.2.10(b), respectively. As expected, the heat distribution in nitrogen and hydrogen behaves the same at low flow rates. Each heat distribution shows a broad maximum between 15 and 20 cm at a temperature of about 50 °C below the heater setpoint. Thus, the sample point was placed at 20 cm. The $Ga(CH_3)_3$ flow rate was fixed at 28.9 μmol/min for all experiments.

Owing to residual hydrocarbons from inside the bubbler and fragments owing to ionization, we compared the relative signal change of the mass spectrum with temperature. Figure 4.1 shows the results for $Ga(CH_3)_3$ in N_2 with the mass spectrum ranging from 5 to 120 u at RT (blue) and 800 ℃ (red). Most fragments are concentrated in the ranges of 14 – 44 u and 69 – 120 u. No further peaks were observed. We then performed a high-resolution scan near each peak. The insert in Fig. 4.1 shows some of the results.

Each value in the unit of u is accurate to three decimal places, which is sufficient to distinguish the components in various gas phases. The measured values are very close to the theoretical values of the gas components, for instance, the peaks at 16.031 u and 15.023 u correspond to CH_4 and CH_3, respectively. Thus we were also able to separate C_2H_4 from N2, which was not possible in previous studies [4 – 9]. Together with C_2H_2, C_2H_3, C_2H_5 and C_2H_6, all CxHy (x, 1 – 3; y, 3 – 8) hydrocarbons were detected.

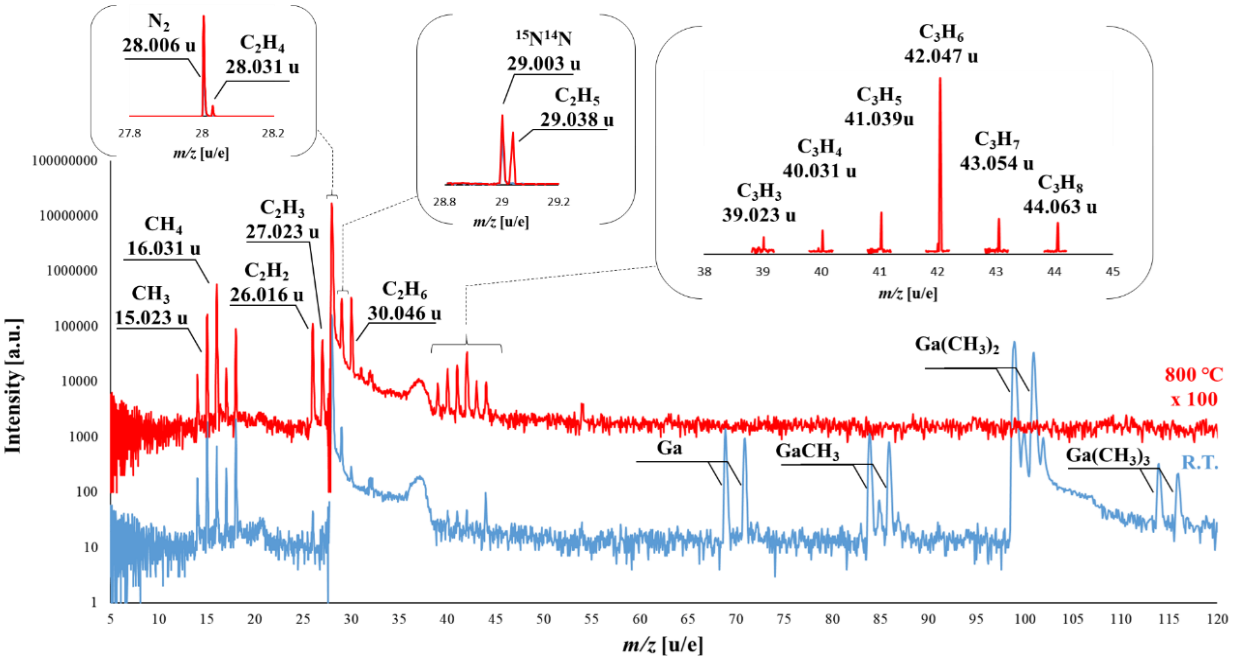

Fig. 4.1 Wide-range mass spectra in N_2 atmosphere at RT (blue) and 800°C (red). The inset shows the high-resolution data for certain masses.

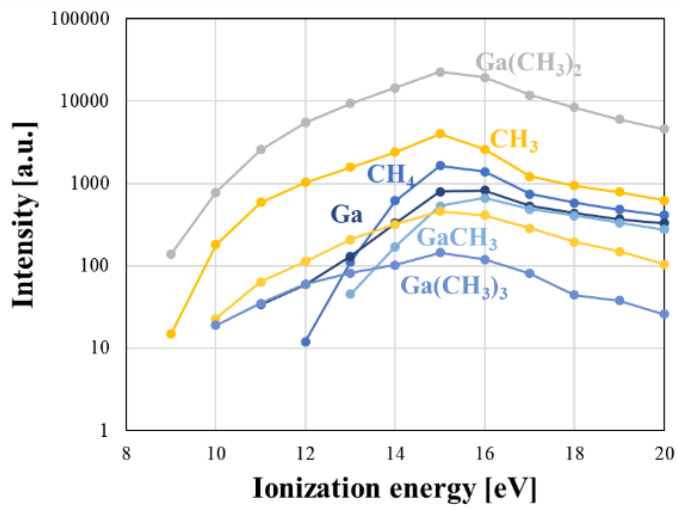

Fig. 4.2 Ionization energy dependence of intensity of Ga- related signals during decomposition of $Ga(CH_3)_3$ at RT

To generate a signal in mass spectrometry, the fragments must be ionized [11]. Choosing an appropriate ionization energy is important, since a must sufficient ionized species without inducing too much fragmentation is necessary. Also, some species may ionize more easily than others. Figure 4.2 shows the effect of ionization voltage on the fragmentation of $Ga(CH_3)_3$ at RT. For all voltages, the signal of $Ga(CH_3)_2$ is much higher than that of Ga(CH3)3, and CH3 was detected even at the low ionization voltages (8 – 12 eV). Thus, $Ga(CH_3)_3$ forms fragments of $Ga(CH_3)_2$ and CH_3 relatively easily upon ionization. It is not yet clear whether this fragmentation can be attributed to the low-probability high-energy tail of electrons [14]. Certainly, a too high ionization voltage (in our case, higher than 15 eV) will cause excessive fragmentation, resulting in at least a

loss of signal, which can also affect the experimental results. Thus, we chose an ionization voltage of 14 eV.

4.3 Results and discussion

Figure 4.3 shows the temperature dependence of the normalized signal intensity of all Ga-related decomposition products in N_2 atmosphere. All decomposition products showed the same dependence, and no other Ga-related decomposition products were generated in the entire temperature range. To verify the results, we performed the same experiments at lower ionization energies and obtained the same results. No intermediate Ga products of $Ga(CH_3)_3$ decomposition were found in the gas phase; if such products existed their lifetimes are too short for their detection or they may attached to the quartz tube surface. Therefore, it is necessary to indirectly analyze the decomposition characteristics of $Ga(CH_3)_3$ through other products in the gas phase. During the ionization, $Ga(CH_3)_2$ had the strongest Ga-related signal (Fig. 4.2); thus, we use it in the following to indicate the amount of undecomposed $Ga(CH_3)_3$.

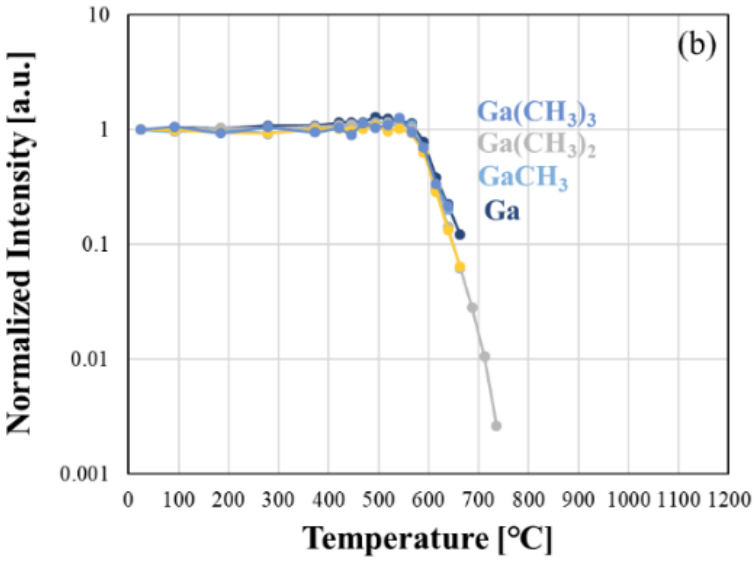

Fig. 4.3 Temperature dependence of Ga-related products during thermal decomposition in N_2 atmosphere, normalized to intensities at RT.

Temperature dependence experiment of TMG decomposition was performed to investigate the decomposition of TMG in nitrogen and hydrogen. Figure 4.4 shows the decomposition results of $Ga(CH_3)_3$ in N_2 and H_2 atmospheres. The $Ga(CH_3)_3$ signal intensity starts to decrease above 520 ℃ in N_2. At the same temperature, the intensity CH_4 and other hydrocarbons (such as C_2H_y) increase. Above 740 ℃, $Ga(CH_3)_3$ is completely decomposed and the signal intensities of most hydrocarbon signals saturate. In H_2 atmosphere, $Ga(CH_3)_3$ begins to decompose above 375 ℃ (which is 150 ℃ lower than the temperature in N_2 atmosphere), and the main product is CH_4. Moreover, the $Ga(CH_3)_3$ is almost completely decomposed at 490 ℃ in H_2 atmosphere, which is 250 ℃ lower than the temperature in N_2 atmosphere. In contrast to the almost inert N_2, H_2

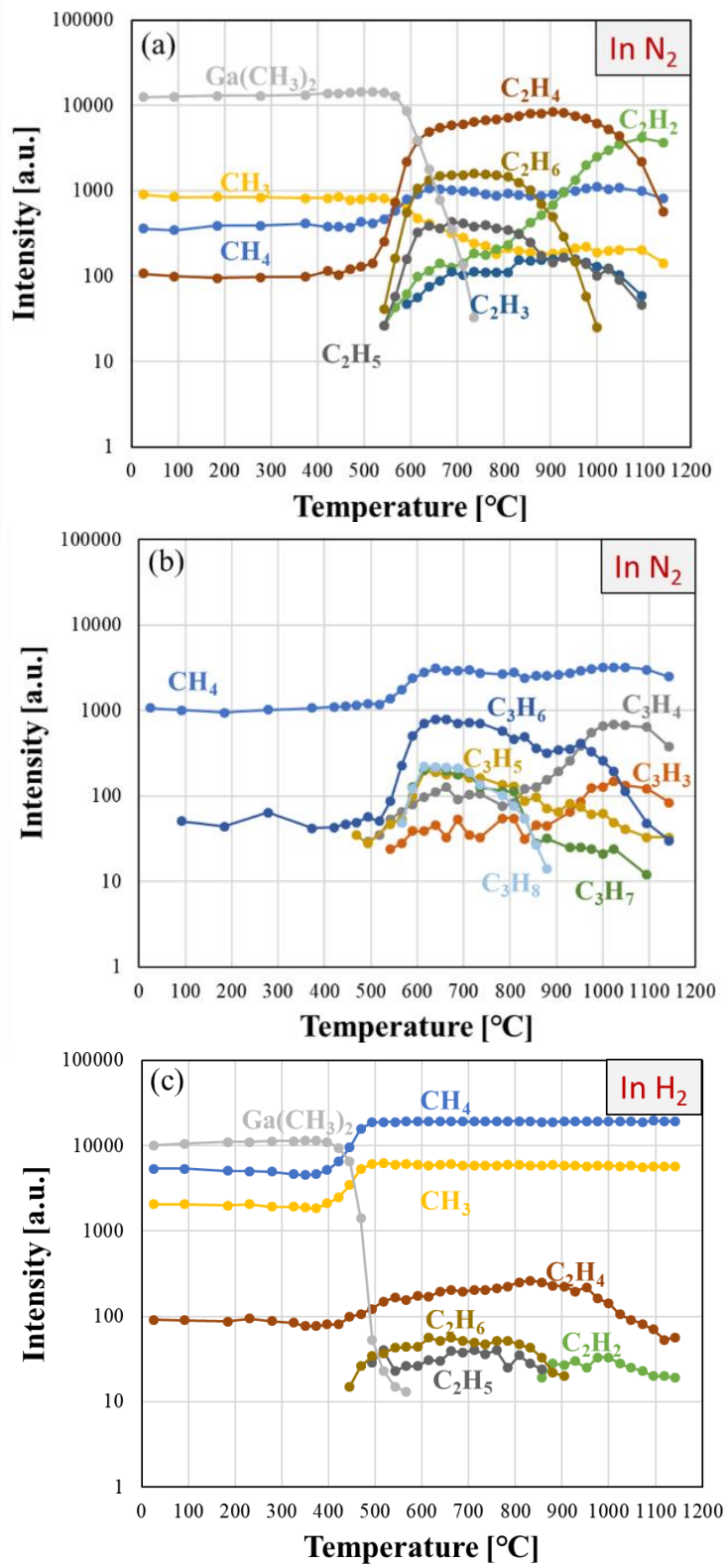

Fig. 4.4 Decomposition results for $Ga(CH_3)_3$: (a) lower hydrocarbons in N_2 atmosphere, (b) higher hydrocarbons in N_2 atmosphere and (c) in H_2 atmosphere.

participates in the reaction. Larsen et al. measured the decomposition of $Ga(CH_3)_3$ in a deuterium D_2 atmosphere, and found a large amount of CH_3D [5,6]. According to the calculation of Kaspari et al., the H_2 carrier gas can produce active H* owing to thermal dissociation above 350 ℃, which is due to the high-energy tail of the Maxwell-Boltzmann distribution [15]. Thus, $Ga(CH_3)_3$ is not decomposed by thermal collision in H_2 atmosphere instead active H* attaches to the CH_3 groups of $Ga(CH_3)_3$ and forms the main product CH_4 above 400 ℃. In contrast, the strong signal of CH_3 suggest that $Ga(CH_3)_3$ lose CH_3* via thermal decomposition in N_2 atmosphere. Schematic diagram of different decomposition processes of TMG in nitrogen and hydrogen was shown in Fig.4.5.

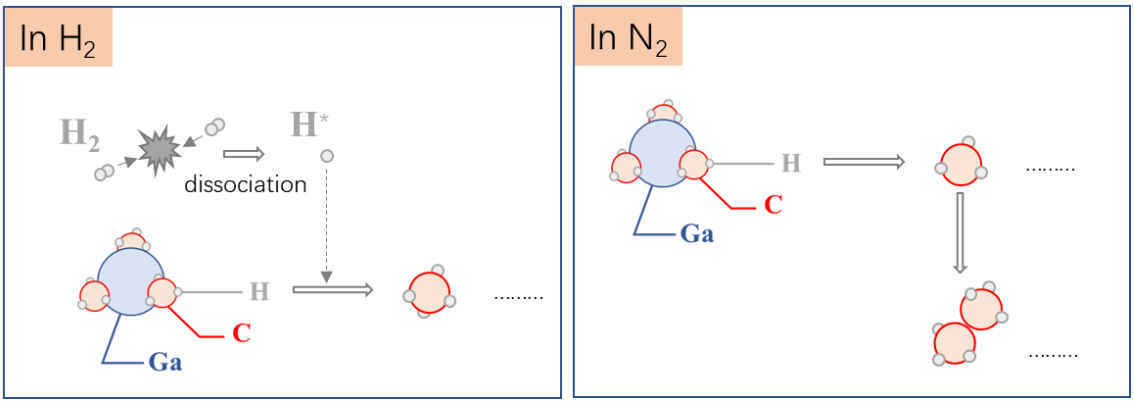

Fig. 4.5 Schematic diagram of different decomposition processes of TMG in nitrogen and hydrogen

The first-principles calculations of Sekiguchi et al. shows that it is possible for TMGa

to be directly decomposed into MMGa [3]. Therefore, C_2H_6 may come from the reaction of two CH3 that are separated from the TMGa decomposition process. The active methyl groups can reacts either with $Ga(CH_3)_3$ or with each other to form the many observed C_2H_y or even larger hydrocarbon (such as C_3H_y at 39 – 44 u and even C_4H_8 at 54 u in Fig. 4.1). Because of their very low signal intensities, they were measured under high-sensitivity conditions, and we used methane as a reference in both Fig. 4.4(a) and 4.4(b). With increasing temperature these hydrocarbons undergo thermal decomposition (pyrolysis) into less saturated hydrocarbons. Thus, the most prominent product is C_2H_4, which is known to form by the thermal cracking of C_2H_6 between 750°C and 900°C. but also, other components appear such as C_3H_4 and C_3H_3 which suggests that many of them are formed and dissociated from CH and CH_2 radicals at high temperatures. However, in the cold environment entry of the TOF-MS system, stable molecules such as CH_4, C_2H_2, C_2H_4 and C_2H_6 dominated over radicals such as CH_3, C_2H_3 and C_2H_5,

Ionization cannot explain the presence of the different hydrocarbons. Although it is known from literature that C_2H_4 are main fragments of C_2H_6 [16,17] and C_2H_2 can be present in high ionization voltage [17]. They predominate only in N_2 in N_2 carrier gas, not in H_2 carrier gas Moreover, the fragmentation of C_2H_6 into C_2H_4 and possible further into C_2H_2 and CH_4 [18,19] during ionization in the TOF-MS system cannot explain the different temperature dependences of those hydrocarbons. However, C_2H_6 can decompose thermally to C_2H_4 and CH_4 below 700 °C [19]. Furthermore, the thermal

decomposition of CH_4 (at high concentrations) to C_2H_6 and C_2H_4 at 725 °C has been observed in a similar setup to ours [20]. Hence, the observed changes of the hydrocarbons are related to thermal decomposition, rather than ionization.

In N_2 atmosphere, the signal intensity of most of the hydrocarbons reacted a maximum at 660 °C, with the exception of CH_3 and C_2H_2 (Fig. 4.4a) and a few other unsaturated hydrocarbons. The signal intensity of CH_3 decreases with decreasing $Ga(CH_3)_3$ signal intensity, which indicates that CH_3 originates from the fragmentation of $Ga(CH_3)_3$ and C_2H_6 in the ionization stage of TOF-MS. The CH_4 signal is relatively weak and is detected at all temperatures. The constant background probably originates from the bubbler, and only the change in intensity is corresponding to the $Ga(CH_3)_3$ decomposition. The formation of CH_4 is clearly not the main pathway of $Ga(CH_3)_3$ decomposition (note the logarithmic scale). Thus, the formed CH_4 is relatively stable and does not have a major role in the reaction. For higher hydrocarbon, we also measured the decomposition of C_2H_6 (Fig. 4.6) in N_2 atmosphere. In the case of pure C_2H_6, the predominant fragment is C_2H_4, even though the decomposition temperature of C_2H_6 is above 660 °C. Indeed, CH_4, which is considered to originate from C_2H_6 decomposition [20], is not observed below 700 °C in Fig. 4.6. Since the intensity ratio of C_2H_4 to C_2H_6 is 3.3 for the decomposition of pure C_2H_6, as well as for $Ga(CH_3)_3$ in N_2 atmosphere below 660 °C, we conclude that most of the C_2H_6 is formed during $Ga(CH_3)_3$ decomposition in N_2 atmosphere. The further decomposition of C_2H_6 to C_2H_4 and then to C_2H_2 only occurs above 660 °C. At typical

GaN growth temperatures of about 1000°C, CH_4 is predominant in H_2 atmosphere, whereas C_2H_2 and C_2H_4 are the main products in N_2 atmosphere at 1000 °C; at higher temperatures, C_2H_2 is the sole products in N_2 atmosphere.

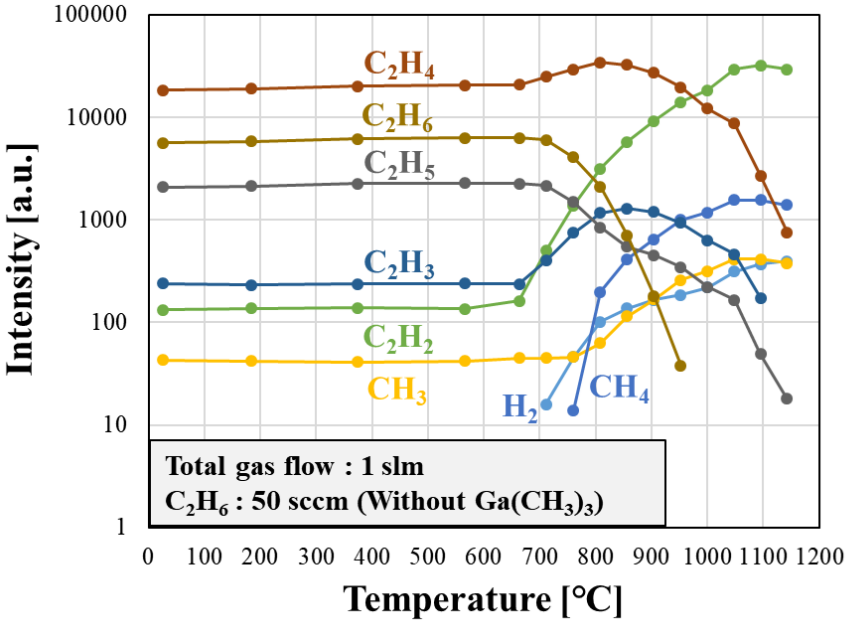

Fig. 4.6 Decomposition results for pure C_2H_6 in N_2 atmosphere.

The above results have consequences in terms of unintentional carbon doping, which can affect the performance of GaN electronic devices [21 – 23]. Hydrocarbons have been intentionally used as carbon dopants for GaN growth [24 – 26]. However, CH_4 has shown very low incorporation efficiency in the literature and is not suitable for intentional doping during GaN MOVPE [24,25]. This is in strong contrast with the high doping efficiency of C_2H_4 and C_2H_2, resulting in their wide use as intentional carbon dopant gases [25,26]. Thus, to reduce the unintentional incorporation of carbon in the GaN growth process, the

formation of C_2H_4 and C_2H_2 should be suppressed. Since the main product of $Ga(CH_3)_3$ decomposition in H_2 is CH_4 as shown in Fig. 4.4(c), some H_2 in the gas phase seems essential.

Figure 4.7 shows the dependence of decomposition products on H_2 content in the gas

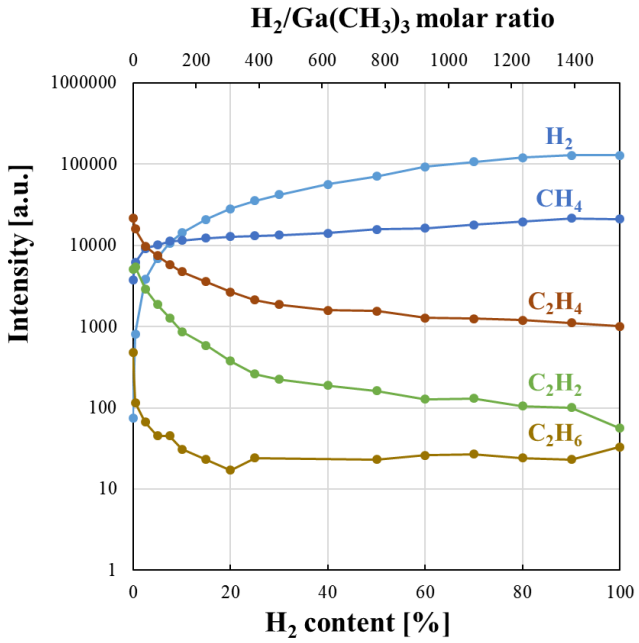

Fig. 4.7 Effect of H_2 content on signal intensity hydrocarbon products at 1000 ℃ in N_2/H_2 atmosphere.

phase at 1000 °C. As the H_2 content increases, the signal intensity of CH_4 increases and those of higher hydrocarbon compounds gradually decrease. In particular, below 20% H_2 (which is a molar ratio of H_2 to $Ga(CH_3)_3$ of 300), the signal intensity of hydrocarbons other than CH_4 significantly increase. Hence, to reduce the hydrocarbon background, a H_2 to $Ga(CH_3)_3$ molar ratio of more than 300 is desirable. Since NH_3 is present during

actual growth, there is already a source of active hydrogen. Assuming NH_3 to be a hydrogen source as efficient as H_2, a V/III ratios of 300 would be required in N_2 atmosphere to avoid the formation of C_2H_y. However, in the actual growth process other reactions may occur; NH_3 may also be a more efficient active hydrogen source than H_2 since other reactions could also affect actual carbon incorporation.

4.4 Summary

We examined the decomposition of trimethylgallium ($Ga(CH_3)_3$) in hydrogen (H_2) and nitrogen (N_2) atmospheres using a high-resolution (about 0.002 u) time-of-flight mass spectrometry system. As a result, we were able to separate N_2 and ethene (C_2H_4) signals. In H_2 atmosphere, the main decomposition product is methane (CH_4) formed by the hydrogenolysis of $Ga(CH_3)_3$. However, in N_2 atmosphere, the main product is ethane (C_2H_6) at temperature lower than 660 °C. Above 660 °C, the C_2H_6 further decomposes into CH_4, acetylene (C_2H_2) and C_2H_4, and the main components in the gas phase are C_2H_2 and C_2H_4 above 1000 ℃. Since these are effective carbon dopants, the molar ratio of H_2 to the $Ga(CH_3)_3$ raw material in the carrier gas should be maintained above 300 to inhibit the formation of hydrocarbons in N_2.

4.5 References

[1] G. B. Stringfellow, "Development and current status of organometallic vapor phase epitaxy," *J. Cryst. Growth*, vol. 264, no. 4, pp. 620–630, 2004.

[2] G.B. Stringfellow, Organometallic vapor-phase epitaxy: theory and practice. 2nd Edition, 1999.

[3] K. Sekiguchi *et al.*, "First-principles and thermodynamic analysis of trimethylgallium (TMG) decomposition during MOVPE growth of GaN," *J. Cryst. Growth*, vol. 468, no. xxxx, pp. 950–953, Jun. 2017.

[4] M. Yoshida and H. Wantanabe, "Mass Spectrometric Study of Ga(CH3)3 and Ga(C2H5)3 Decomposition Reaction in H2 and N2," *J. Electrochem. Soc. Solid-State Sci. Technol.*, vol. 132, no. 3, pp. 677–679, 1985.

[5] C. A. Larsen, N. I. Buchan, and G. B. Stringfellow, "Reaction mechanisms in the organometallic vapor phase epitaxial growth of GaAs," *Appl. Phys. Lett.*, vol. 52, no. 6, pp. 480–482, 1988.

[6] C. A. Larsen, N. I. Buchan, S. H. Li, and G. B. Stringfellow, "Decomposition mechanisms of trimethylgallium," *J. Cryst. Growth*, vol. 102, no. 1–2, pp. 103–116, Apr. 1990.

[7] P. W. Lee, T. R. Omstead, D. R. McKenna, and K. F. Jensen, "In situ mass spectroscopy studies of the decomposition of organometallic arsenic compounds in the presence of Ga(CH3)3 and Ga(C2H5)3," *J. Cryst. Growth*, vol. 93, no. 1–4, pp. 134–142, 1988.

[8] J. O. Williams, R. D. Hoare, O. Khan, M. J. Parrott, D. J. Cole-Hamilton, and R. J. M. Griffiths, "Mechanisms in Metal-Organic Chemical Vapour Deposition [and Discussion]," *Philos. Trans. R. Soc. A Math. Phys. Eng. Sci.*, vol. 330, no. 1610, pp. 183–193, 1990.

[9] M. Mashita, "Reaction mechanisms in the omvpe growth of gaas and algaas," *Jpn. J. Appl. Phys.*, vol. 29, no. 5 R, pp. 813–819, 1990.

[10] A. R. Date and A. L. Gray, "Plasma source mass spectrometry using an inductively coupled plasma and a high resolution quadrupole mass filter,"

Analyst, vol. 106, no. 1269, pp. 1255–1267, 1981.

[11] K. Nagamatsu *et al.*, "Decomposition of trimethylgallium and adduct formation in a metalorganic vapor phase epitaxy reactor analyzed by high-resolution gas monitoring system," *Phys. Status Solidi Basic Res.*, vol. 254, no. 8, pp. 1–4, 2017.

[12] S. Shimma, H. Nagao, J. Aoki, K. Takahashi, S. Miki, and M. Toyoda, "Miniaturized high-resolution time-of-flight mass spectrometer MULTUM-S II with an infinite flight path," *Anal. Chem.*, vol. 82, no. 20, pp. 8456–8463, 2010.

[13] Z. Ye *et al.*, "Ammonia decomposition and reaction by high-resolution mass spectrometry for group III – Nitride epitaxial growth," *J. Cryst. Growth*, vol. 516, no. March, pp. 63–66, Jun. 2019.

[14] N. BAHLAWANE, F. REILMANN, L. SALAMEH, and K. KOHSEHOINGHAUS, "Mass-Spectrometric Monitoring of the Thermally Induced Decomposition of Trimethylgallium, Tris(tert-Butyl)Gallium, and Triethylantimony at Low Pressure Conditions," *J. Am. Soc. Mass Spectrom.*, vol. 19, no. 7, pp. 947–954, Jul. 2008.

[15] C. Kaspari, M. Pristovsek, and W. Richter, "Deoxidation of (001) III–V semiconductors in metal-organic vapour phase epitaxy," *J. Appl. Phys.*, vol. 120, no. 8, p. 085701, Aug. 2016.

[16] Y. Amenomiya and R. F. Pottie, "Mass spectra of some deuterated ethanes. I. The effect of ionizing voltage," *Can. J. Chem.*, vol. 46, no. 10, pp. 1735–1739, May 1968.

[17] R. Stockbauer, "Threshold electron-photoion coincidence mass spectrometric study of CH 4, CD4, C2H6, and C 2D6," *J. Chem. Phys.*, vol. 58, no. 9, pp. 3800–3815, May 1973.

[18] S. Popović, S. Williams, and L. Vušković, "Electron-impact dissociative ionization of ethylene," *Phys. Rev. A - At. Mol. Opt. Phys.*, vol. 73, no. 2, p. 022711, Feb. 2006.

[19] M. C. Lin and M. H. Back, "THE THERMAL DECOMPOSITION OF ETHANE: PART II. THE UNIMOLECULAR DECOMPOSITION OF THE ETHANE MOLECULE AND THE ETHYL RADICAL," *Can. J. Chem.*, vol. 44,

no. 20, pp. 2357–2367, Oct. 1966.

[20] C. Chen, M. H. Back, and R. A. Back, “The Thermal Decomposition of Methane. I. Kinetics of the Primary Decompositionto C 2 H6 + H 2 ; Rate Constant for the Homogeneous Unimolecular Dissociation of Methane and its Pressure Dependence,” *Can. J. Chem.*, vol. 53, no. 23, pp. 3580–3590, Dec. 1975.

[21] T. Kachi, “Recent progress of GaN power devices for automotive applications,” *Jpn. J. Appl. Phys.*, vol. 53, no. 10, 2014.

[22] N. A. Fichtenbaum, T. E. Mates, S. Keller, S. P. DenBaars, and U. K. Mishra, “Impurity incorporation in heteroepitaxial N-face and Ga-face GaN films grown by metalorganic chemical vapor deposition,” *J. Cryst. Growth*, vol. 310, no. 6, pp. 1124–1131, 2008.

[23] P. Gamarra, C. Lacam, M. Tordjman, J. Splettstösser, B. Schauwecker, and M. A. Di Forte-Poisson, “Optimisation of a carbon doped buffer layer for AlGaN/GaN HEMT devices,” *J. Cryst. Growth*, vol. 414, pp. 232–236, 2015.

[24] M. R. Ramdani, M. Chmielowska, Y. Cordier, S. Chenot, and F. Semond, “Effect of carbon doping on crystal quality, electrical isolation and electron trapping in GaN based structures grown silicon substrates,” *Solid. State. Electron.*, vol. 75, pp. 86–92, 2012.

[25] X. Li, Ö. Danielsson, H. Pedersen, E. Janzén, and U. Forsberg, “Precursors for carbon doping of GaN in chemical vapor deposition,” *J. Vac. Sci. Technol. B, Nanotechnol. Microelectron. Mater. Process. Meas. Phenom.*, vol. 33, no. 2, p. 021208, Mar. 2015.

[26] N. Koide, T. Hikosaka, Y. Honda, M. Yamaguchi, and N. Sawaki, “Incorporation of carbon on a (1 1̄0 1) facet of GaN by MOVPE,” *J. Cryst. Growth*, vol. 284, no. 3–4, pp. 341–346, 2005.

Chapter 5 Reactions in TMGa / NH_3 system

5.1 Background

In the MOVPE growth mode, TMGa and NH_3 are used as gallium precursor and nitrogen precursor for GaN, respectively. Compared with the complex reaction of directly detecting the actual growth, the measurement of the individual decomposition process of each raw material have be done. We have found some interesting results, such as the main production of C_2H_6 during the thermal decomposition of TMG. Controlling the ratio of H_2 and TMG can control the formation of hydrogen carbon compounds. However, since NH_3 is present during actual growth, there is already a source of active hydrogen. Assuming NH3 to be a hydrogen source as efficient as H_2, a V/III ratios of 300 would be required in N_2 atmosphere to avoid the formation of C_2Hy（y:2-6）. However, in the actual growth process other reactions may occur; NH_3 may also be a more efficient active hydrogen source than H2 since other reactions could also affect actual carbon incorporation. In 1996, Thon et al., used ND_3 and D_2 to mark the GaN gas phase reaction process. In TMG/H_2/ND_3 system, CH_3D was found. It is means TMG can react with NH_3. And then, In TMG/D_2/NH_3, failed to produce CH_3D, with only CH_4 found in the product stream [1]. The literature suggests that NH_3 may be more active than H_2.

In summary, in the presence of NH_3, the detection of the TMGa decomposition reaction will provide more comprehensive information for us to further understand the formal

reaction inside the reactor. Therefore, this section focuses on the experimental results of TMGa and NH_3 under different conditions.

5.2 Experimental

The experimental setup is the same as before, and all reaction processes take place inside the tubular pathway. The heating range is 30cm. After the gases are fully heated, the reactions between them will be more sufficient. This helps our observation. In the actual crystal growth process, the V/III ratio is controlled above 1,000. However, an excessive amount of NH_3 may cause the change to be insignificant, while an excessively small amount of NH_3 will cause the change to be too rapid and difficult to observe. Therefore, in the experiments in this section, in order to better observe the gas-phase reaction process, the V/III ratio is controlled at 100, and the total flow rate and the TMG flow rate are consistent with the previous experiments.

5.3 The reaction between NH_3 and TMGa

Because TMGa decomposes quickly in hydrogen and the main reactant is CH_4. Considering that it is not easy to see the effect of NH_3 on the decomposition of TMG in hydrogen, we investigated the effect of NH_3 on the decomposition of TMG in a nitrogen atmosphere.

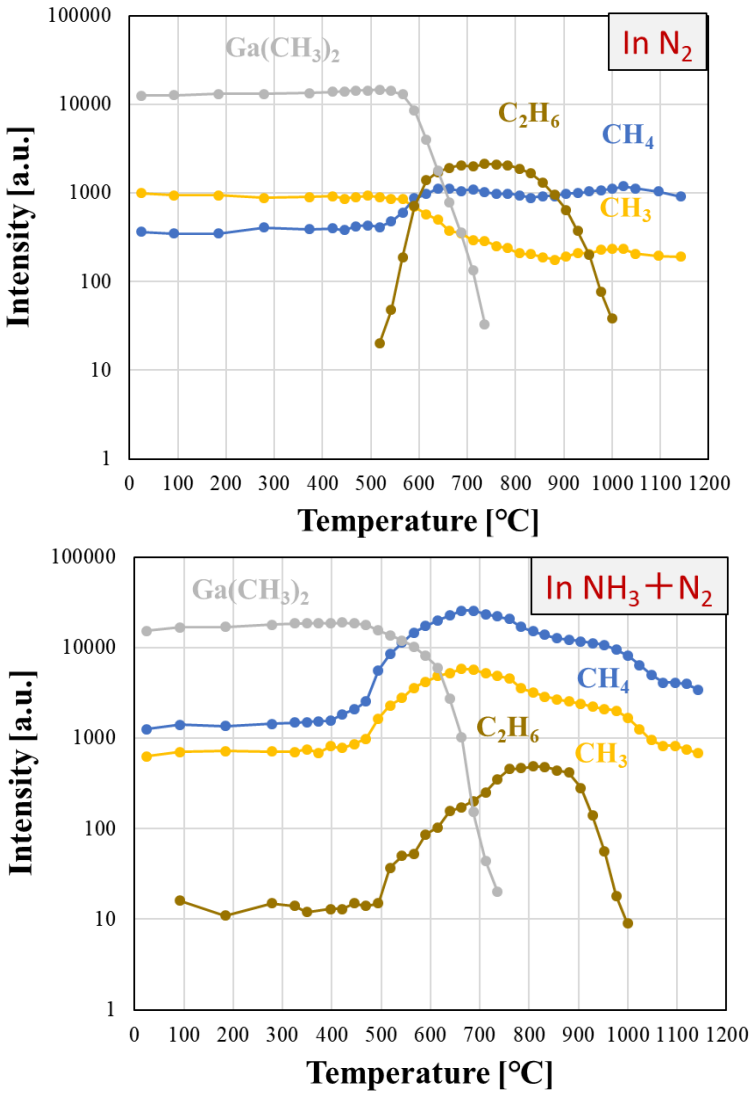

Fig. 5.1 TMG decomposition in N_2 and in NH_3+N_2

The different decomposition result of TMGa in N_2 and NH_3(with N_2) was shown in Fig.5.1. It is only a preliminary observation of the reaction of TMGa and NH_3. All the representative DMGa, CH_4, C_2H_6 are used to compare the effect of NH_3 on the decomposition of TMGa. First, the strength of CH_4 and C_2H_6 has changed over 500°C.

Due to the addition of NH_3, a large amount of CH_4 is generated, while The signal strength of C2H6 is obviously weakened. According to the literature [1], NH_3 provides effective active H atoms. Therefore, CH3 from TMGa will preferentially form CH_4 in react with active H, rather than C2H6. Secondly, both CH_4 and C_2H_6 show a rapid decrease in high temperature regions over over 700℃. However, due to the stable nature of its tetrahedral structure, CH_4 is almost not expected to react in the gas phase. This is because at high temperatures, hydrogen carbon compounds (even CH_4) will react with ammonia to form HCN. Details about HCN will be introduced in the next 5.4 section The final obvious change is that the decomposition of TMGa is accelerated due to the activity of NH_3, and the final result shows that the decomposition temperature of TMGa is reduced， it shows that NH_3 can promote the decomposition reaction of TMGa

5.2 The decomposition of NH_3 and Ga metal catalyst

Because the NH_3 reaction is not as complicated as the decomposition of TMGa. Understanding the gas phase reaction from the perspective of NH_3 is also a way. NH_3 decomposition in different condition is shown in Fig,5.2.

Each heat distribution shows a broad maximum between 15 and 20 cm at a temperature of about 50°C below the heater setpoint. Thus, the sample point was placed at 20 cm, basically, NH_3 flow was kept in 50 sccm.

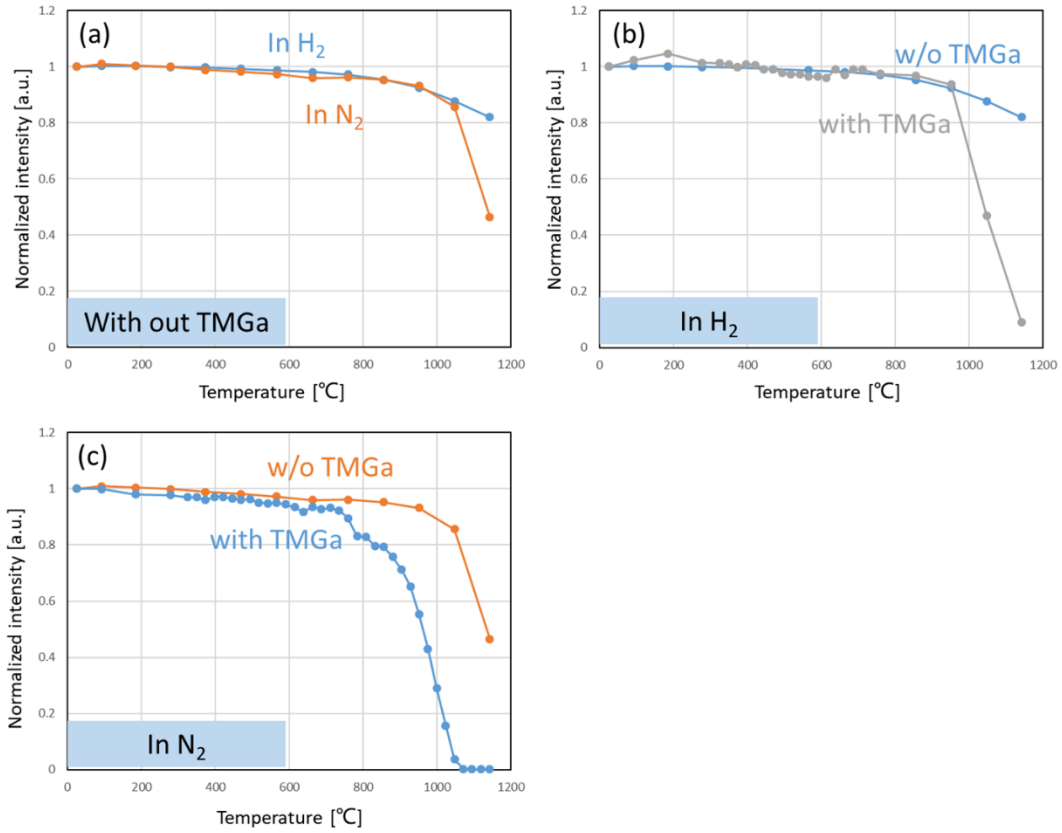

Fig. 5.2 NH_3 decomposition in different condition

Decomposition efficiency of ammonia in hydrogen and nitrogen as basic comparative data is shown in Fig.5.2 (a). Although the thermodynamic analysis of ammonia shows the possibility of complete decomposition at 400 ℃, in fact ammonia decomposition is a sluggish reaction [2]. NH_3 is not at equilibrium state in MOVPE reactor due to high flow speed. According to our results, even at a low flow rate of 0.03 m/s, the decomposition of NH_3 under 800 ℃ is very weak. When it exceeds 1000 ℃, we can see very obvious NH_3 decomposition changes, and then it is even more obvious that NH_3 exhibits

completely different decomposition rates under different carrier gases. As shown, the decomposition rate of ammonia in nitrogen is significantly higher than that in hydrogen. According to the literature [6], the decomposition of NH_3 is a process of gradual dehydrogenation. However, as mentioned in the previous chapter, a large number of active hydrogen atoms exist due to thermal collisions in hydrogen [3]. Therefore, hydrogen suppresses the decomposition of NH_3. We also compared the decomposition of ammonia in different carrier gases in the presence of TMGa. Figure 5.2 (a) shows the comparison of NH_3 decomposition with and without TMGa in H_2. And Fig 5.2 (b) shows those of in N_2. Due to the presence of TMGa, the decomposition of ammonia in the high temperature region is significantly accelerated, even in a hydrogen atmosphere. However, according to the current experimental conditions, even the decomposition from NH_3 is due to the reaction with TMGa. Only 1% of NH_3 is consumed. Therefore, in the presence of TMGa, the reason for the large amount of ammonia decomposition needs to be explained. In my point of view, it is because the decomposition of NH_3 is accelerated due to the action of Ga metal catalyst. Organometallics generate metal droplets in the final thermal decomposition stage. There are also many studies on the catalytic effect of ammonia, and metal catalysts in those are the most widely used [4-8]. Because ammonia is not only used in nitride semiconductors, it also has important research significance in the fields of agriculture, chemical industry, fuel cells, and so on [6]. It can also be seen that even under the catalyst effect, the inhibitory effect of H_2 influences the decomposition

of NH_3. At a high temperature of 1000 ℃, ammonia is only about 10% in a hydrogen atmosphere, while the decomposition rate of hydrogen in a nitrogen environment is as high as 70%. However, the catalytic effect of Ga metal is very difficult to measure directly, because Ga and NH_3 will block the progress of the GaN formed on the surface. In the presence of TMGa, the decomposition data of NH_3 in nitrogen is shown in Fig.5.2(c). The data in the figure shows that NH_3 starts to decompose at about 750 degrees. This is because TMGa generates a large amount of hydrogen carbon compounds such as C_2H_6 in nitrogen, which reacts with ammonia to form HCN preferentially than CH4.

According to the current data, the conclusions I can give in this section are as follows: first, H_2 inhibits the decomposition of ammonia, and second, the presence of Ga catalyst causes a large amount of NH_3 decomposition

5.4 Analysis of HCN formation reaction

Compared with the separate thermal decomposition process, the decomposition products of TMGa show a very unstable trend in the presence of ammonia. Both CH_4 and C_2H_6 show a rapid decrease in high temperature regions as shown in Fig 5.2. Due to the stable nature of CH_4, we repeated the experiments carefully and all showed the same results. Eventually we found an unreported peak near m / z = 27. Detailed analysis results show that the exact mass of this substance is 27.011u. Inferred from the mass of each chemical

atom, the substance is a combination of one H atom (1.008 u), one C atom (12 u), and one N atom(14.003 u). Therefore, we can basically judge that HCN is generated during the reaction.

HCN was found in both hydrogen and nitrogen processes, and its comparative data is shown in Fig. 5.3a. Through comparison, we find that HCN is mainly generated in the temperature region above 700 ℃. So HCN is unlikely from the reaction directly with NH_3 and TMGa. Because, even decomposes relatively slowly in a nitrogen atmosphere, TMGa is basically completely decomposed at 700 ℃ under the same experimental conditions. We also found that HCN formation is slower and requires higher temperatures in hydrogen. Considering that the main decomposition product of TMGa in hydrogen is CH_4, the reaction of CH_4 and NH_3 needs to be explored. Kachel et al. used FTIR to analyze the reaction of CH_4 and NH_3 [9]. They found that the first HCN signal in FTIR spectrum was recorded at 800 ℃ without Pt, while it appeared already at 600 ℃ for experiments with Pt. Obviously, the catalyst effect not only improves the decomposition efficiency of NH_3, but also affects the activation of NH_3. Comparing their HCN generation results without metal catalyst, our TOF test data shows a higher decomposition rate (even comparing their HCN generation results with Pt). Therefore, in the gas phase reaction of nitrides, due to the catalytic action of Ga metal, a high reaction mode of CH_4 and NH_3 is established.

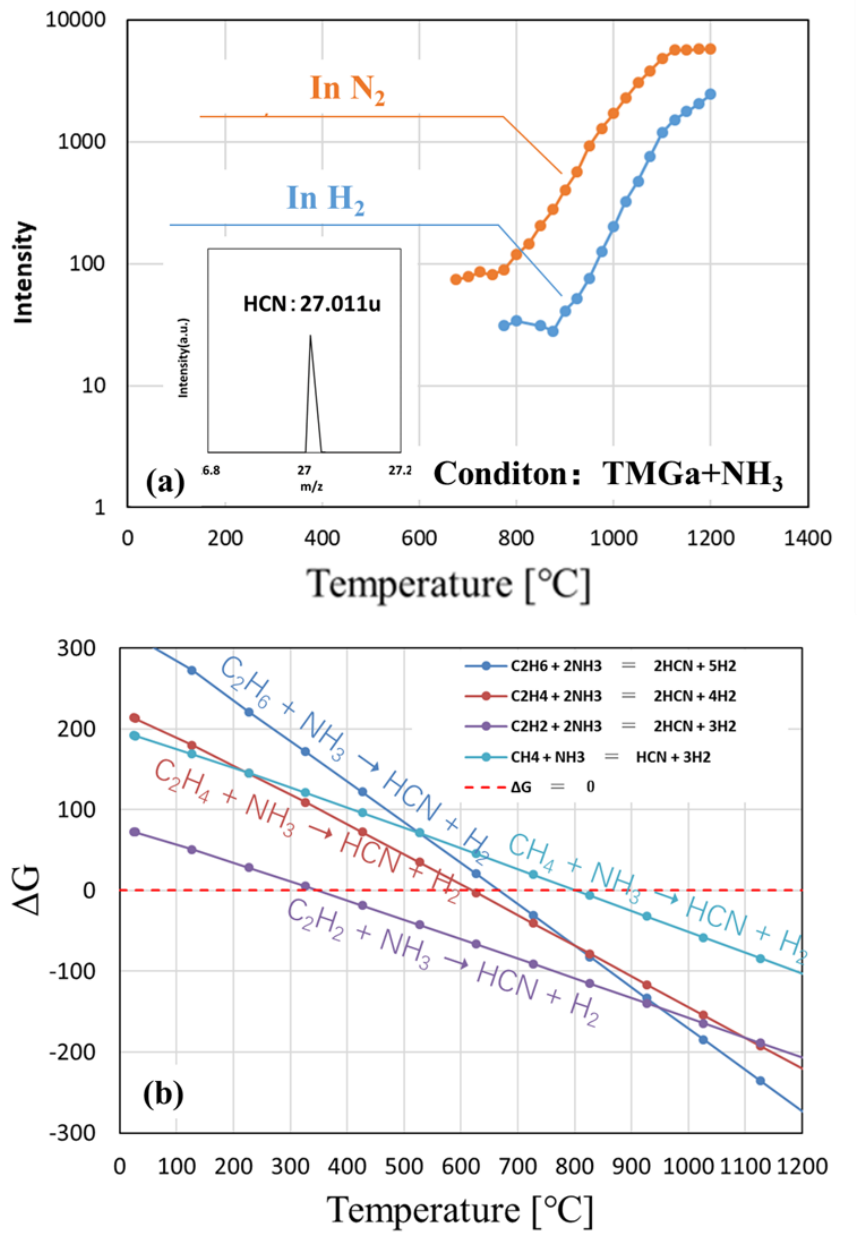

Fig. 5.3 HCN generation at different carrier gas (a) and the related thermodynamic explanations (b)

According to our results, the formation temperature of HCN in nitrogen is lower than the reaction in a hydrogen atmosphere. This is because the process of TMGa in nitrogen generates a large amount of hydrocarbon compounds, Gadzhiev et al. show that C_2H_2,

C_2H_4, etc. have a high probability of forming HCN from ammonia by quantum chemical study [10]. Both HCN and C_2H_2 are highly toxic and are not suitable for a more detailed discussion in a simple reactor [10]. Thermodynamic calculations can help us understand these reactions. We considered the following four ways of reaction, related thermodynamic data from NIST-JANAF Thermochemical Tables.

$$CH_4 + 2NH_3 \rightarrow 2HCN + 3H_2 \qquad (5.1)$$

$$C_2H_6 + 2NH_3 \rightarrow 2HCN + 5H_2 \qquad (5.2)$$

$$C_2H_4 + 2NH_3 \rightarrow 2HCN + 4H_2 \qquad (5.3)$$

$$C_2H_2 + 2NH_3 \rightarrow 2HCN + 3H_2 \qquad (5.4)$$

Thermodynamic calculation results are shown in the Fig 5.3b. The reaction of methane and ammonia is thermodynamically shown as 800 ℃, which is highly consistent with our experimental results in H_2. C_2H_6 and other thermodynamic calculations show that they react more easily with NH_3 than CH_4, It is also consistent with our observations in a N_2 atmosphere. The observations in the previous chapter show that C_2H_6 will decompose to generate C_2H_4 at about 660 ℃. However, the study in this chapter shows that the decomposition of C_2H_6 into C_2H_4 is unlikely to occur, because at about 660 ℃, C_2H_6 will react with NH_3 to generate HCN.

HCN is not only highly toxic but can also be used as a carbon doping material for GaN. While calling on all operators of nitride crystal growth to pay more attention to safety, whether HCN is the main source of unintentional carbon doping needs to be carefully explored. However, as shown in Fig 5.3, The signal intensity of HCN increases with increasing temperature, which means that as the temperature increases, the concentration of HCN in the gas phase increases. Even at high temperatures of 1200 ° C, HCN shows very stable characteristics and will not undergo more decomposition. However, increasing temperature is an effective means to reduce the incorporation of caobon impurities in GaN. So even if we detect a high content of HCN at high temperature, it is obviously not directly related to the actual crystal growth results.

5.5 TMG decomposition temperature shifted by carrier gas

In the previous chapter we found that the decomposition temperature of TMGa is different in different carrier gases. Detailed comparison results will be collated in this section. The decomposition results of TMGa under different gas environments are shown in Figure 5.4. In nitrogen, due to the reaction of TMGa and NH_3, the decomposition temperature of TMGa is significantly reduced. However, in hydrogen, the related temperature changes show the opposite trend. The results showed that the addition of ammonia gas caused the TMG decomposition temperature phase to shift by about 50 degrees in the high temperature direction. H_2 promotes TMGa decomposition, NH_3

inhibits decomposition. Relevant experiments have been confirmed repeatedly. Thon et al. also tested the same results in a hydrogen atmosphere [1]. They explain the effect due to the formation of TMGa: NH_3 adduct. But we did not observe any signs of adduct in the experiments. We speculate that it may also be related to the suppression of NH_3 decomposition by H_2. However, the explanation of TMGa decomposition temperature shift in hydrogen is not clear enough at present.

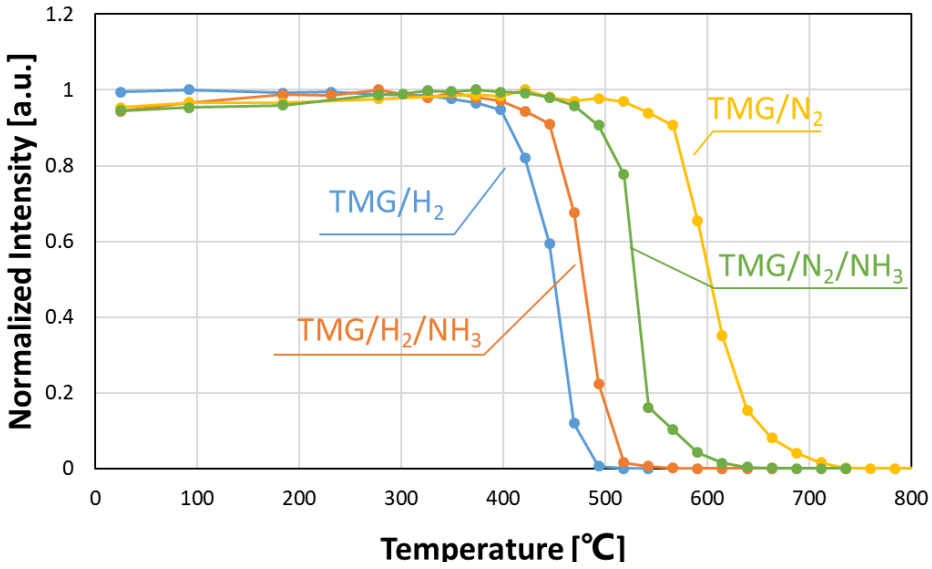

Fig. 5.4 TMGa decomposition temperature shifted at different carrier gas.

5.6 Discussion on flow rate and reaction decomposition rate

In the actual growth process, the flow velocity in reactor is very high, and the heating zone is very short, so when the heat energy required for the reaction or decomposition is not enough, the real reaction in actual reactor may be mainly the reaction in the relatively

low temperature region we observed. Therefore, it is necessary to analyze the reaction at different flow rates.

Due to equipment limitations, the flow rate can be increased up to 10 slm (flow rate 0.2m / s) for convenient experiments. For comparison experiments, the partial pressures of all imported materials（NH_3, MO, carrier gas） remain unchanged. The gas phase temperature has been measured in advance.

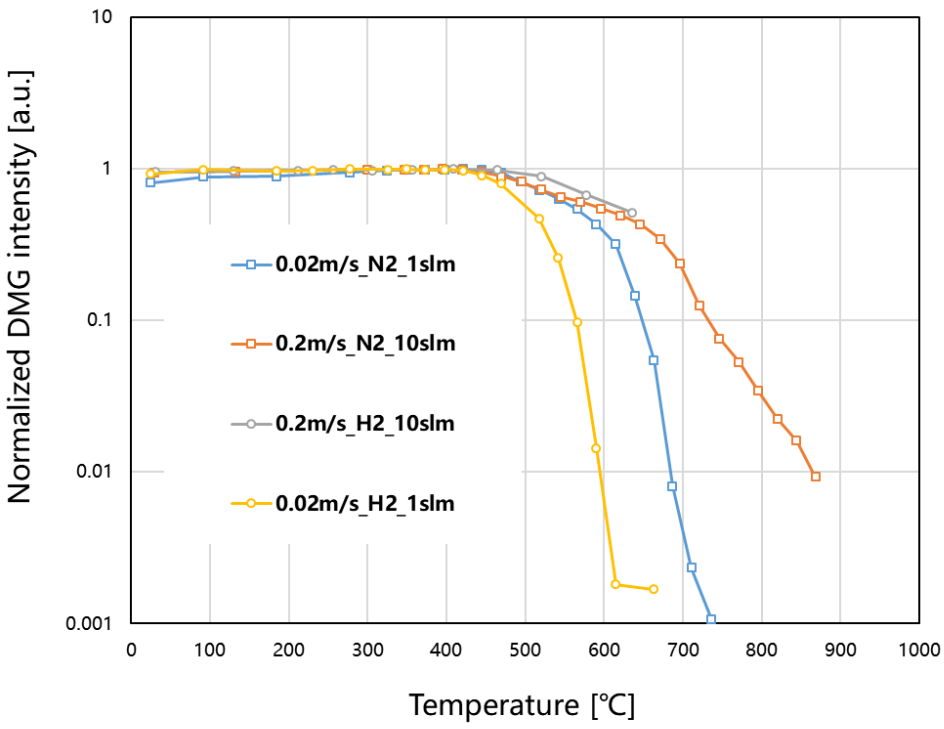

Fig. 5.5 Discussion on flow rate for TMG

The comparison results at different flow rates are shown in Figure 5.5. The corresponding initial decomposition temperatures at all flow rates are about the same,

indicating that the temperature control in our experiments is accurate and the results are credible. The overall decomposition curve shows that at high flow rates, the decomposition will move in the direction of high temperature (even near 1000 ℃). These indicate that, in fact, the decomposition reaction of TMGa will not be “fast”, and in addition to the temperature, the reaction time will be required. Therefore, the degradation behavior of TMG at high flow rates appears to be a slow response. Experimental conditions on our simple reactor have a heating area of 30 cm and a flow rate of only 0.2 m / s. However, in the actual growth reactor, the flow velocity can reach several m / s, and the heating zone of the furnace is generally not long.

So from the perspective of the trend, at high flow rates, a large amount of raw materials that are not completely decomposed will appear near the substrate and directly cause the incorporation of carbon.

5.5 References

[1] A. Thon and T. F. Kuech, “High temperature adduct formation of trimethylgalliu m and ammonia,” *Appl. Phys. Lett.*, vol. 69, no. 1, pp. 55–57, Jul. 1996.

[2] K. Sunwoon *et al.*, “The influence of ammonia pre-heating to InGaN films grown by TPIS-MOCVD,” *J. Cryst. Growth*, vol. 247, no. 1–2, pp. 55–61, 2003.

[3] C. Kaspari, M. Pristovsek, and W. Richter, “Deoxidation of (001) III–V semiconductors in metal-organic vapour phase epitaxy,” *J. Appl. Phys.*, vol. 120, no. 8, p. 085701, Aug. 2016.

[4] H. Shindo, C. Egawa, T. Onishi, and K. Tamaru, “Reaction mechanism of ammonia decomposition on tungsten,” *J. Chem. Soc. Faraday Trans. 1 Phys. Chem. Condens. Phases*, vol. 76, pp. 280–290, 1980.

[5] R. E. Burk, “The Thermal Decomposition of Ammonia upon the Surface of a Molybdenum Wire,” *Proc. Natl. Acad. Sci.*, vol. 13, no. 2, pp. 67–74, Feb. 1927.

[6] S. F. Yin, B. Q. Xu, X. P. Zhou, and C. T. Au, “A mini-review on ammonia decomposition catalysts for on-site generation of hydrogen for fuel cell applications,” *Appl. Catal. A Gen.*, vol. 277, no. 1–2, pp. 1–9, Dec. 2004.

[7] S. Kenichi, D. Hironaga, A. Mihara, A. Hashimoto, and A. Yamamoto, “Catalyst Temperature Dependence of NH 3 Decomposition for InN Grown by Metal Organic Vapor Phase Epitaxy,” *Jpn. J. Appl. Phys.*, vol. 52, no. 08, p. 08JD04, 2013.

[8] W. Arabczyk and J. Zamlynny, “Study of the ammonia decomposition over iron catalysts,” *Catal. Letters*, vol. 60, pp. 167–171, 1999.

[9] W. Arabczyk and U. Narkiewicz, “A new method for in situ determination of number of active sites in iron catalysts for ammonia synthesis and decomposition,” *Appl. Surf. Sci.*, vol. 196, no. 1–4, pp. 423–428, 2002.

[10] G. Ertl and M. Huber, “Mechanism and kinetics of ammonia decomposition on iron,” *J. Catal.*, vol. 61, no. 2, pp. 537–539, 1980.

[11] O. B. Gadzhiev *et al.*, “The role of NH3 and hydrocarbon mixtures in GaN pseudo-halide CVD: a quantum chemical study,” *J. Mol. Model.*, vol. 20, no. 11,

p. 2473, Nov. 2014.

[12] K. Kachel, D. Siche, S. Golka, P. Sennikov, and M. Bickermann, “FTIR exhaust gas analysis of GaN pseudo-halide vapor phase growth,” *Mater. Chem. Phys.*, vol. 177, pp. 12–18, Jul. 2016.

Chapter 6 Conclusions and Future Outlook

With the increasing application prospects of Group-III nitride semiconductor, the principle of crystal growth needs to be elaborated. Although the crystal quality can be improved by optimizing the crystal growth conditions, the reaction inside the reactor is still unclear. To the realization of high-quality materials for extended nitride semiconductors application, so more accurate mechanism elucidation than before is essential. The main objective of this research is to explore specific processes in gas phase reactions of GaN MOVPE.

A simple reactor was built to make experiments more convenient. In the MOVPE growth mode, TMGa and NH_3 are used as gallium precursor and nitrogen precursor for GaN, respectively. Compared with the complex reaction of directly detecting the actual growth, the measurement of the individual decomposition process of each raw material is more helpful to our understanding of the MOVPE reaction mode. The decomposition process of NH_3 under nitrogen was observed first. The decomposition of ammonia (NH_3) in nitrogen (N_2) ambient was studied under non-equilibrium conditions similar to those in a metal organic vapor phase epitaxy (MOVPE) reactor during the epitaxial growth of group-III nitrides. The gas phase was sampled at different positions and analyzed using a time-of-flight mass spectrometry system with a high resolution (better than 0.002 u). Our results expand earlier findings. Even at the high temperature of 1200°C, only 26% of NH3

decomposed in a clean metal-free reactor, whereas a higher ratio of NH3 decomposition was realized in the presence of stainless steel. The activation energy in the clean reactor was calculated to be 0.965 ± 0.004 eV. Subsequently, we followed the decomposition of TMGa in H_2 and N_2 atmosphere. Thus, we could separate N_2 and ethene (C_2H_4) signal. In H2, the main product is $CH_4$by hydrogenolysis for $Ga(CH_3)_3$. However, in N_2, the main product is C_2H_6 at lower temperature. From 600°C on C_2H_6 will further decompose into CH_4, C_2H_2 and C_2H_4 until the main component in gas phase becomes C_2H_2 and C_2H_4 above 1000 ℃. Since these are effective carbon dopants, the molar ratio of H_2 to $Ga(CH_3)_3$ raw material should be maintained above 300 in the carrier gas to inhibit the formation of hydrocarbon compounds in N_2. the decomposition process of TMGa under different carrier gases was studied. TMGa begins to decompose in hydrogen (H_2) and nitrogen (N_2) at 375 and 520 °C, respectively. In contrast to the almost inert N_2, H_2 participates in the reaction. the H2 carrier gas can produce active H* owing to thermal dissociation above 350 ℃, which is due to the high-energy tail of the Maxwell-Boltzmann distribution. Therefore, TMGa is not decomposed by thermal collision in H2 atmosphere instead active H* attaches to the CH_3 groups of $Ga(CH_3)_3$ and forms the main product CH_4 above 400 ℃. In contrast, the strong signal of CH_3 suggest the $Ga(CH_3)_3$ lose CH_3* via thermal decomposition in N_2 atmosphere. Specifically, in the nitrogen atmosphere, with the decomposition of TMGa, we observed high-intensity signal of hydrocarbons compounds such as C_2H_6 and C_2H_4. Finally, by introducing pure C_2H_6, TMGa was proved

preferentially generates C_2H_6 during the thermal decomposition process. We also observed that C_2H_6 will continue to decompose into C_2H_4 and C_2H_2 at high temperatures. However, In the presence of NH_3, hydrocarbon compounds (even CH_4) will react with NH3 to form HCN. This type of reaction mode was first reported to occur during the gas phase reaction of nitrides. HCN is not only highly toxic but can also be used as a carbon doping material for GaN. While calling on all operators of nitride crystal growth to pay more attention to safety, whether HCN is the main source of unintentional carbon doping needs to be carefully explored. However, by comparing the reactions at different flow rates, We eventually found that unintentionally doped carbon sources were more likely to come from undecomposed MO.

The simple reaction experimental system we set up can carry out experiments very conveniently. As a result, I have figured out most of the reaction modes in the gas phase and found new reaction paths. Using such basic data as a basis, further theoretical analysis and optimization of nitrides can be developed. The significance of this study has been achieved. We explore the gas phase beginning of the entire crystallization reaction to provide accurate and detailed theoretical data for the subsequent development of nitrides. However, the actual reaction process is in a non-equilibrium state at high flow rates. Our device cannot reach conditions close to the actual growth environment. Therefore, the strategic position of this research is to help everyone know what happens in the gas phase of the reactor. The biggest challenge is to figure out how the reactions that have been

determined will change in real growing environments as specific conditions change. For the future development of this research, testing in an actual growth reactor is an essential process. Paired with optical detection equipment, the analysis of gas phase and crystal surface while growing may obtain more critical data.

Acknowledgments

Firstly, I would like to thank my supervisor Prof. Hiroshi Amano for giving me such great opportunity to study in Nagoya University. The Ph.D course at the Amano laboratory has been the most valuable time of my life. Because of his kindness concern and pertinent advices, I could learn a lot of things ranging from scientific knowledge to enthusiasm as a researcher.

I'd like to thank all the reviewers of my Ph. D (Prof. Shiraishi, Prof. Kumagai, Prof. Ohno). Thanks for taking the time to help me review my thesis and give me the opportunity to learn more about my research. Also, I would also like to thank Prof. Yoshio Honda who carefully advises me on research fields. I can get advice from him on the nature of one problem every time. I also really thank Professor Pristovsek Markus for the selfless help.

Special thanks are given to Prof. Nitta. Without his encouragement, my life is another look I did not expect. I respect him from my heart.

The research cannot be carried out smoothly without the support of all aspects. Thank Inoue san and Kojima san (TOMOE SHOKAI Co.,LTD) for the supply of gaseous raw materials. Thank nakashima san (MSI.TOKYO, Inc.) and nagao san (Atonarp, Inc.) for the guidance on Tof-MS. Thank Takahashi san (THREE.S Co.,LTD.)for his help with device modification. I appreciate all secretaries very much for their help in daily affairs.

I would like to thank Professor Atsushi Tanaka, Assistant Professor Maki Kushimoto, Assistant Professor Manato Deki and all members in Amano Lab for the Laboratory daily.

Finally, I want to thank my family. The forgiving love from them is my most precious treasure.

Sincerely wish everyone health and well-being

Ye

Achievement List

A. Publications

1) Zheng Ye, Shugo Nitta, Yoshio Honda, Markus Pristovsek, Hiroshi Amano, "Analysis of the gas-phase reaction of TMG and NH_3", (Article in preparation).

2) Zheng Ye, Shugo Nitta, Yoshio Honda, Markus Pristovsek, Hiroshi Amano, "Analysis of Trimethylgallium Decomposition by High-Resolution Mass Spectrometry", (In press, https://doi.org/10.35848/1347-4065/ab6fb0).

3) Zheng Ye, Shugo Nitta, Kentaro Nagamatsu, Naoki Fujimoto, Maki Kushimoto, Manato Deki, Atsushi Tanaka, Yoshio Honda, Markus Pristovsek, Hiroshi Amano, "Ammonia Decomposition and Reaction by High-Resolution Mass Spectrometry for Group III-Nitrides Epitaxial Growth", Journal of Crystal Growth, 516, 63-66 (2018).

4) Kentaro Nagamatsu, Yuto Ando, Zheng Ye, Ousmane 1 Barry, Atsushi Tanaka, Manato Deki, Shugo Nitta, Yoshio Honda, Markus Pristovsek, Hiroshi Amano, "Comparing high-purity c- and m-plane GaN layers for Schottky barrier diodes grown homoepitaxially by metalorganic vapor phase epitaxy", Japanese Journal of Applied Physics, 57, 105501 (2018).

5) Kentaro Nagamatsu, Shugo Nitta, Zheng Ye, Hirofumi Nagao, Shinichi Miki, Yoshio Honda, Hiroshi Amano,"Decomposition of trimethylgallium and adduct formation

in a metalorganic vapor phase epitaxy reactor analyzed by high-resolution gas monitoring system", Physica Status Solidi (B) Basic Research, Vol.254, No.8, pp.1-4 (2017).

6) Zheng Sun, Akio Ohta, Seiichi Miyazaki, Kentaro Nagamatsu, Hojun Lee, Marc Olsson, Zheng Ye, Manato Deki, Yoshio Honda, Hiroshi Amano, "The interface analysis of GaN grown on 0° off 6H-SiC with an ultra-thin buffer layer", Japanese Journal of Applied Physics, Vol.55, No.1, p.010303 (2016).

B. International Conference Presentation

1) Yuto Okawachi, Kenta Chokawa, Masaaki Araidai, Akira Kusaba, Yoshihiro Kangawa, Koichi Kakimoto, Zheng Ye, Yoshio Honda, Shugo Nitta, Hiroshi Amano, Kenji Shiraish, "Theoretical Study of the Origins of Carbon Impurities on GaN MOVPE from a Gas Phase Reaction Perspective ~Incorporation of Ga and C Related Molecules~", The 9th Asia-Pacific Workshop on Widegap Semiconductors, November 10-15, Okinawa (Japan), (2019).

2) Yuto Okawachi, Kenta Chokawa, Masaaki Araidai, Akira Kusaba, Yoshihiro Kangawa, Koichi Kakimoto, Zheng Ye, Yoshio Honda, Shugo Nitta, Hiroshi Amano, Kenji Shiraish, "Study of the Origins of Carbon Impurities on Gallium Nitride MOVPE from a Gas Phase Reaction Perspective", International Conference on Materials and

Systems for Sustainability, November 1-3, Nagoya (Japan), (2019).

3) Yuto Okawachi, Kenta Chokawa, Masaaki Araidai, Akira Kusaba, Yoshihiro Kangawa, Koichi Kakimoto, Zheng Ye, Yoshio Honda, Shugo Nitta, Hiroshi Amano, Kenji Shiraish, “Study of the Origins of Carbon Impurities on GaN MOVPE from a Gas Phase Reaction Perspective”, The 19th International Conference on Crystal Growth and Epitaxy, July 28 - August 2, Colorado (USA), (2019).

4) Zheng Ye, Shugo Nitta, Kentaro Nagamatsu, Naoki Fujimoto, Maki Kushimoto, Manato Deki, Atsushi Tanaka, Yoshio Honda, Markus Pristovsek, Hiroshi Amano, “Ammonia Decomposition and Reaction by High-Resolution Mass Spectrometry for Group III-Nitrides Epitaxial Growth”, The 19th International Conference on Metalorganic Vapor Phase Epitaxy, June 3-8, Nara(Japan), (2018).

5) Shugo Nitta, Zhibin Liu, Shigeyoshi Usami, Zheng Ye, Kentaro Nagamatsu, Maki Kushimoto, Manato Deki, Atsushi Tanaka, Yoshio Honda, Markus Pristovsek, Hiroshi Amano, “In situ and ex situ optical characterization of nitride semiconductor crystal for advanced optical and power electronic devices”, Optics 2017, November 14-17, Las Vegas, (USA), (2017).

6) Kentaro Nagamatsu, Yuto Ando, Zheng Ye, Ousmane 1 Barry, Atsushi Tanaka, Manato Deki, Shugo Nitta, Yoshio Honda, Markus Pristovsek, Hiroshi Amano, “Reduction of impurities and realization of high breakdown voltage Schottky barrier

diodes using homoepitaxial m-plane GaN grown", The 12th International Conference on Nitride Semiconductors, July 24-28, Strasbourg (France), (2017).

7) Shugo Nitta, Kentaro Nagamatsu, Miyagoshi Ryosuke, Zheng Ye, Yoshio Honda, Hiroshi Amano, "Reduction of impurities and realization of high breakdown voltage Schottky barrier diodes using homoepitaxial m-plane GaN grown", International Workshop on Nitride Semiconductors, October 2-7, Orland (USA), (2016).

8) Kentaro Nagamatsu, Shugo Nitta, Zheng Ye, Hirofumi Nagao, Shinichi Miki, Yoshio Honda, Hiroshi Amano, "Decomposition of trimethyl gallium in a metal organic vapor-phase epitaxy reactor using an in-line high-resolution gas monitoring system", International Workshop on Nitride Semiconductors, October 2-7, Orland (USA), (2016).

9) Xu Yang, Shugo Nitta, Kentaro Nagamatsu, Yuhuai Liu, Zheng Sun, Zheng Ye, Junya Matsushita, Yoshio Honda, Hiroshi Amano, "Influence of residual boron on the crystal quality of GaN films grown by MOVPE", International Workshop on Nitride Semiconductors, October 2-7, Orland (USA), (2016).

10) Manato Deki, Zheng Ye, Yoshio Honda, Hiroshi Amano, "Characterization of Deep States in GaN SBDs Grown by MOHVPE Using Photo-Capacitance Spectroscopy", The 6th International Symposium on Growth of III-Nitrides, November 8-12, Hamamatsu (Japan), (2015).

11) Zheng Sun, Peifeng Song, Zheng Ye, Marc Olsson, Manato Deki, Yoshio Honda,

Hiroshi Amano, “Pre-Al Treatment Influence for GaN Growth on SiC with an Ultrathin Buffer Layer”, The 6th International Symposium on Growth of III-Nitrides, November 8-12, Hamamatsu(Japan), (2015).

12) Zheng Ye, Zheng Sun, Kentaro Nagamatsu, Manato Deki, Yoshio Honda, and Hiroshi Amano, “Pre-Al Treatment Influence for GaN Growth on SiC with an Ultrathin Buffer Layer”, The 6th International Symposium on Growth of III-Nitrides, November 8-12, Hamamatsu (Japan), (2015).

13) Zheng Sun, Marc Olsson, Zheng Ye, Tsutomu Nagayama, Tetsuya Wataneba, Yoshio Honda, Hiroshi Amano, “Mg-ion-implantation Damage Influence on the Lattice Deformation of GaN”, The 7th Asia-Pacific Workshop on Widegap Semiconductors, May 17-20, Seoul (Korea), (2015).

C. Domestic Conference Presentation

1) 大河内 勇斗, 長川 健太, 洗平 昌晃, 草場 彰, 寒川 義裕, 柿本 浩一, 叶 正, 本田 善央, 新田 州吾, 天野 浩, 白石 賢二, “気相反応の観点から見たGaN MOVPE中の炭素混入の原因の解明”, 電子デバイス界面テクノロジー研究会 - 材料・プロセス・デバイス特性の物理 - , 1月31日-2月1日, 静岡(日本), (2020).(Accepted).

2) Yuto Okawachi, Kenta Chokawa, Masaaki Araidai, Akira Kusaba, Yoshihiro

Kangawa, Koichi Kakimoto,Zheng Ye, Yoshio Honda, Shugo Nitta, Hiroshi Amano, Kenji Shiraish, “第一原理計算と熱力学的解析によるGaN MOVPE成長中の炭素取り込みの考察”, ポスト「京」重点課題(7) 第5回シンポジウム「次世代の産業を支える新機能デバイス・高性能材料の創成(CDMSI)」, 8月9日, 東京(日本), (2019).

3) 叶 正, 新田 州吾, 永松 謙太郎, 本田 善央, 天野 浩, “高分解能質量分析によるIII族窒化物半導体気相成長のためのアンモニア分解及び反応の解析”, 第65回応用物理学会春季学術講演会,3月17日-20日, 東京(日本), (2018).

4) 叶 正, 新田 州吾, 永松 謙太郎, 本田 善央, 天野 浩, “III族窒化物半導体有機金属気相成長におけるアンモニアの反応モニタリング”, 第12回シリコンフロンティア研究会, 1月12日, 名古屋(日本), (2018).

5) 叶 正, 永松 謙太郎, 新田 州吾, 本田 善央, 天野 浩, “MOHVPE法における中間反応”, 第64回応用物理学会春季学術講演会, 3月14日-17日, 横浜(日本), (2017).

6) 叶 正, 永松 謙太郎, 久志本 真希, 出来 真斗, 新田 州吾, 本田 善央, 天野 浩, “MOHVPE装置のフローチャネル部材材質に対するHClの耐腐食性”, 第5回結晶工学未来塾,11月7日, 東京農工大学(日本), (2016).